NANOFRABICATION AND CHARACTERIZATION

OF SILVER NANOPARTICLES

TAY BING YUAN

BACHELOR OF SCIENCE (HONS) CHEMISTRY

FACULTY OF SCIENCE

UNIVERSITI TUNKU ABDUL RAHMAN

MAY 2019

NANOFRABICATION AND CHARACTERIZATION

OF SILVER NANOPARTICLES

BY

TAY BING YUAN

A project submitted to the Department of Chemical Science

Faculty of Science

Universiti Tunku Abdul Rahman

In partial fulfilment of the requirements for the degree of

Bachelor of Science (Hons) Chemistry

May 2019

ABSTRACT

Owing to small size effect and large surface area, silver nanoparticle (AgNPs) exhibits special physical properties and is widely used in different applications. One of the significant applications is that AgNPs are coated on the surface of solar cell to increase the light harvesting efficiency of solar cell due to its localized surface plasmon resonance (LSPR) effect. AgNPs could be synthesized through chemical reduction method using silver nitrate as metal precursor, sodium borohydride as reducing agent while 1-dodecanthiol as capping agent. In this study, the effects of the concentration of reducing agent, the concentration of capping agent and reaction temperature on the formation of AgNPs in term of size and shape had been studied and investigated. The synthesized AgNPs were characterized using UV/Vis spectroscopy, Fourier-transform infrared spectroscopy spectrophotometry (FTIR), and X-ray diffraction (XRD), while the surface morphology of AgNPs was studied using scanning electron microscopy (SEM), atomic force microscopy (AFM) and light microscope (LM). The smaller AgNPs with average size of 20-70 nm could be synthesized with an optimum concentration of $NaBH_4$ of 0.36 M (R value = 18), the concentration of DDT of 0.052 M (S value = 0.5) and at 0 $^{\circ}$C. The coupling agent, 3-(Trimethoxysilyl)-1-propanethiol (MPTMS) was used as the adhesion promoter to deposit the AgNPs on the surface of solar cell. By coating AgNPs on the surface of solar cell, the greatest improvement of light harvesting efficiency was 108.8 % with 0.136 W.

ABSTRAK

Disebabkan kesan saiz kecil dan kawasan permukaan yang besar, nanopartikel perak (AgNPs) mempamerkan sifat fizikal khas dan luas digunakan dalam pelbagai aplikasi. Salah satu aplikasi yang penting adalah AgNP yang disalut pada permukaan sel suria untuk meningkatkan kecekapan penuaian cahaya sel solar akibat kesan resonans plasmon permukaan tempatan (LSPR). AgNPs boleh disintesis melalui kaedah pengurangan kimia menggunakan perak nitrat sebagai pendahulu logam, natrium borohidrida sebagai agen mengurangkan manakala 1-dodecanthiol sebagai agen penutup. Dalam kajian ini, kesan kepekatan ejen pengurangan, kepekatan ejen pelindung dan suhu reaksi terhadap pembentukan AgNPs dalam bentuk saiz dan bentuk telah dikaji dan disiasat. AgNP disintesis dicirikan menggunakan spektroskopi UV/Vis, spektroskopi inframerah Fourier-transform (FTIR), dan X-ray difraksi (XRD), manakala morfologi permukaan AgNPs dikaji dengan menggunakan mikroskop elektron scanning (SEM), mikroskopi daya atom (AFM) dan mikroskop cahaya (LM). AgNPs yang lebih kecil dengan saiz purata 20-70 nm boleh disintesis dengan kepekatan optimum NaBH$_4$, 0.36 M (R value = 18), kepekatan DDT, 0.052 M (S = 0.5) dan pada 0 ^{o}C. Ejen gandingan, 3-(trimethoxysilyl)-1-propanethiol (MPTMS) digunakan sebagai promoter lekatan untuk mendepositkan AgNPs pada permukaan sel suria. Dengan lapisan AgNPs pada permukaan sel solar, peningkatan kecekapan penuaian cahaya adalah 108.8% dengan 0.136 W.

ACKNOWLEDGEMENT

First and foremost, I would like to express my sincere gratitude to my final year project supervisor, Dr. Chee Swee Yong for her patience, enthusiasm, motivation, immense knowledge and most importantly her unceasing support for my final year project. Her guidance assisted me a lot in completing the research and thesis.

Apart from that, I would like to address my appreciation to my friends, lab mates and lab officers for the thought-provoking discussion and assists me for completion of research and thesis. Indeed, they have provided a friendly and cooperative work environment as well as useful feedback and insightful comments on my work. Moreover, I would like to thank my family members for their unconditional support, both financially and emotionally throughout my degree.

Last but not least, my deepest appreciation was addressed to Universiti Tunku Abdul Rahman (UTAR) for providing me a comfortable environment and sufficient advanced facilities to carry out my final year project.

DECLARATION

I hereby declare that the project report is based on my original work except for quotations and citations which have been duly acknowledged. I also declare that it has not been previously or concurrently submitted for any other degree at UTAR or other institutions.

_____

(TAY BING YUAN)

APPROVAL SHEET

This project report entitled **"NANOFRABICATION AND CHARACTERIZATION OF SILVER NANOPARTILCES"** was prepared by **TAY BING YUAN** and submitted as partial fulfilment of the requirements for the degree of Bachelor of Science (Hons) Chemistry at Universiti Tunku Abdul Rahman.

Approved by:

_____

(Dr. CHEE SWEE YONG)   Date: ………………………

Supervisor

Department of Chemical Science

Faculty of Science

Universiti Tunku Abdul Rahman

FACULTY OF SCIENCE

UNIVERSITI TUNKU ABDUL RAHMAN

Date: _____

PERMISSION SHEET

It is hereby certified that **TAY BING YUAN** (ID No: **15ADB03106**) has completed this final year project entitled **"NANOFRABICATION AND CHARACTERIZATION OF SILVER NANOPARTILCES"** under the supervision of **Dr. CHEE SWEE YONG** from the Department of Chemical Science, Faculty of Science.

I hereby give permission to the University to upload the softcopy of my final year project in pdf format into the UTAR Institutional Repository, which may be made accessible to the UTAR community and public.

Yours truly,

_____

 (TAY BING YUAN)

TABLE OF CONTENTS

LIST OF TABLES

LIST OF FIGURES

LIST OF ABBRREVIATIONS

AEAPTMS   N-[3-(Trimethoxysilyl)propyl]ethylenediamine

AFM   Atomic force microscopy

Ag   Silver

AgNPs   Silver nanoparticles

$AgNO_3$ Silver nitrate

ATR   Attenuated total reflectance

Au   Gold

^oC Degree celcius

C.A.   Volume % of coupling agent

cm   Centimeter

Cu   Copper

DC   Direct current

DDT   1-Dodecanethiol

FCC   Face centred cubic

FTIR   Fourier-transform infrared spectroscopy

ICDD   International Centre for Diffraction Data

kV   kilo-voltage

LBL   Layer-by-layer

LM   Light microscope

LSPR   Localized surface plasmon resonance

M   Molar

mA	Mili-ampere
min	Minute
mL	Milliliter
mW	Mili-watt
MPTMS	3-(Trimethoxysilyl)-1-propanethiol
N	Nitrogen
$NaBH_4$	Sodium borohydride
nm	Nanometer
NPs	Nanoparticles
O	Oxygen
$-OCH_3$	Methoxy group
P	Phosphorus
p-n junctions	Positive and negative junctions
PV	Photovoltaic
R-O	Alkoxy group
rpm	Revolutions per minute
S	Sulphur
SEM	Scanning electron microscopy
Si	Silicon
SOI	Thin-silicon-on-insulator
UV-Vis	UV-Visible spectrophotometry
V	Voltage
v	Volume

v/v %	Volume per volume percent
XRD	X-ray diffraction
º	Degree
%	Percent

CHAPTER 1

INTRODUCTION

1.1   Nanoparticles

Nanoparticles are a wide class of materials which are defined as the tiny solid particles with the size ranges from 1 to 100 nm, and surrounded by an interfacial layer. In fact, nanoparticles are complicate molecules which consist of three layers: surface layer (interfacial layer), shell layer and core. The interfacial layer can be functionalized with different tiny molecules, stabilizers or surfactants, and polymers. On the other hands, the core, basically is the center element of the nanoparticles and is always referred to the nanoparticle itself. The shell layer is a chemically different substance compared to the core in all aspects (Khan and Saeed, 2017). Bulk substances with large particle size possess of constant physical properties, such as boiling point, freezing point, and color of materials, disregarding to its size. However, the properties of the particles at nanoscale are depending on their size. Therefore, when the particle size gets closer to nanoscale, their properties will alter significantly with the increase in the total surface area (Mavani and Shah, 2013).

Nowadays, nanoparticles have attracted the attention of many scientists. This is because nanoparticles exhibit significant physical and chemical properties due to their nano-size effect and large total surface area. Thus, nanoparticles are widely applied in various fields, for example, solar cell, optical devices, industrial catalyst, cancer therapy, food and electronic packaging, waste water treatment etc. (Zaman, et al., 2014). Classification of nanoparticles depends on the particle size, chemical and physical properties, dimension of structure and morphology. The examples of some well-known nanoparticle categories are metallic nanoparticles, polymeric nanoparticles, carbon- and lipid-based nanoparticles, ceramic nanoparticles, and semiconductor nanoparticles (Khan and Saeed, 2017).

1.1.1 Metallic nanoparticles

Metallic nanoparticles are purely synthesized from the metal precursors. In the past few decades, metal nanoparticles had receive a vast attentions from scientists due to the remarkable exciting electronic and optical properties, optoelectrical properties which are resulted by well-known localized surface plasmon resonance (LSPR) with its extraordinary size-dependent properties (Khan, 2017). Metallic nanoparticles have large surface-area-to-volume ratio as compared to the bulk equivalents, localized surface plasmon resonance (LSPR) frequency is very dependent on the size, shape and dielectric nature of nanoparticles interface with the surrounding environment. Nanoparticles are advantageously used in developing of electro-optical device, substrates for enhancing Raman spectrophotometer,

chemical and biological detector, and matter for high capacity storage media. Moreover, the special and unique properties of nanoparticles such as chirality, catalysis, large surface energies, electrochemical characteristics, photoluminescence, plasmon excitation and quantum confinement have resulted in their exploitation in several applications in different fields (Swami, et al., 2004). For example, DNA sequencing, drug delivery, single electron tunneling devices, UV blocking textile, cell imaging, interactive food, activated carbon filter, water disinfection etc. (Cheah, et al., 2015).

Alkali and noble metal nanoparticles such as copper (Cu), silver (Ag) and gold (Au) have received extensive attention compared to the other metal nanoparticles. They have been extensively studied by applying capping agent (stabilizer) as a protecting group such as alkanethiol or mecaptan, polymer, and ligands. Among these three noble metal nanoparticles, Ag and Au are well studied compared to Cu due to their properties of high particles stability because they are less susceptibility to oxidation reaction which resulted in less formation of oxide layer.

1.1.2 Synthesis of silver nanoparticle

Silver nanoparticles (AgNPs) are the particles of silver, with particle size between 1 and 100 nm. While often described as being 'silver', a part of them are composed of an extensive percentage of silver oxide because of their large ratio of surface to bulk silver atoms. In various fields, silver nanoparticles are synthesized and constructed in different shapes, depending on the application at hand. Silver nanoparticles are becoming an increasingly important matter in many technologies. They exhibit the highest efficiency of plasmon excitation compared to other metallic nanoparticles. Silver nanoparticles are the only matter whose plasmon resonance can be tuned to different wavelength in visible spectrum (Mirela n.d.).

There are two general approaches to synthesize the AgNPs, namely top-down and bottom-up approaches. The bottom-up approach is more preferable by scientist in synthesizing narrow nanoparticles with narrow size distribution. This approach is literally referring to construction of a matter from bottom (atom, molecule and cluster). The principle of molecular self-assembly and molecular recognition are applied and utilized by bottom-up approach. By using chemical properties of single molecule, the molecule components are either self-organizing into favorable conformation or relying on positional assembly. Bottom-up approach involves depletion of matter components with further self-assembly process and resulted in the formation of nanostructures. Physical forces applied on nanostructure are mainly for combining the nanoscale units into large stable structures. The examples

of bottom-up approach are quantum dot and the formation of NPs through colloidal dispersion (Harish, et al., 2018).

On the other hand, top-down approach is one of microfabrication methods, including macroscopic structures which can be externally controlled using tools to cut, mill, and shape materials into desiderated order and shape during the processing of nanostructures. The typical examples of top-down approach are attrition or milling, and vapor treatment which is a top-down secondary approach to engineer nanostructures (Saghaei, et al., 2016). The difference between top-down and bottom-up approaches is that top-down approach begins with the generation of a pattern on a large scale, and reduced to nanoscale. It is quick to manufacture but slow and unsuitable for large scale production. However, bottom-up approach starts with molecules or atoms and forming nanostructures. This kind of nanofabrication is cheaper (Harish, et al., 2018).

1.1.3   Localized surface plasmon resonance (LSPR)

Localized surface plasmon resonance (LSPR) is defined as the charge density oscillation confined to metallic nanostructure. It is an optical phenomenon which occurs when the light wave trapped inside the conductive nanoparticles is smaller than the light wavelength. This phenomenon is generated by the interaction between incident light and surface electrons in conduction band. The particular interaction results in coherent localized plasmon oscillations with a resonant

frequency, as shown in Figure 1.1. The intensity and resonant frequency have a strong correlation with separation distance between nanoparticles, size, size distribution, composition, dielectric constant of surrounding, geometry and electronic structure of nanoparticles (Petryayeva and Krull, 2011).

When the metal nanoparticles are excited by absorbing the light of a certain frequency, an electromagnetic field is created, resulting in coherently oscillation of free electrons in conduction bands of the metal. The charge is separated and a dipole oscillation with the parallel direction axis to electric field of light occurs due to the electrons oscillation behavior on the surface of such particles. The maximum amplitude at certain oscillation frequency generates LSPR effect (Elnoby, et al., 2018). The localized field is enhanced and more incident light is scattered into the absorber layer. The noble metal nanoparticles have stronger LSPR compared to other metal nanoparticles. The resonance wavelength for most of the noble metal nanoparticles locates within visible and infrared regions (Barman, et al., 2018).
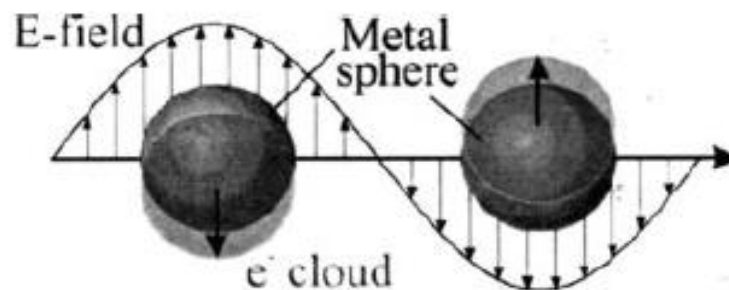
Figure 1.1: A schematic diagram represents LSPR where free electrons in metal nanoparticles interact with incident light and resulted in plasmon oscillation (Hutter and Fendler, 2004).

1.2 Capping agent

Capping agent is also known as stabilizer or surfactant, which acts as the protecting group to prevent and restrict the particles from aggregation, agglomeration and over-growth during the synthesis of nanoparticles. Capping agents are frequently used in nanoparticle synthesis to interface with metal nanoparticles in order to limit and control the size, shape, physiochemical properties and structural characteristics of metal nanoparticles. By forming of surfactant layer during the particle growth process, the reaction kinetics can be regulated (Phan and Hoang, 2017). Several mechanisms are applied by capping agent when functioning, which include steric and electrostatic stabilization, stabilization by van der Waals and hydration forces and depletion stabilization (Ajitha, et al., 2016).

Stabilizers are usually amphiphilic molecules which contain a hydrophilic head (polar group) and a hydrophobic tail (non-polar group). The functionality of the stabilizer depends upon both polar head and non-polar tail. The polar head will coordinate to the center metal atom of nanoparticles while non-polar tail will interact with the surrounding medium. The hydrophilic head consists of donor atoms (P, S, O and N) with functional groups. The donor atoms carry un-pair electrons which are capable of forming coordinate or dative bonds with metal atoms (Gulatil, et al., 2018). Thiolate capping agent has been proved to be a suitable ligand used as protecting agent in the synthesis of AgNPs due to the strong covalent nature of Ag-S interaction.

1.3   Silane coupling agent

Silane coupling agents are the compounds contain of two or more different reactive functional groups in a molecule structure which are capable in forming a strong chemical bond (coupling) between two dissimilar materials or organic and inorganic materials. Silane coupling agents are widely utilized in several fields because they are able to bind the organic materials with different polarity of materials such as alumina surface and inorganic silica. Silane coupling agents are normally applied to function as an adhesion promoter to improve the physical properties of composite materials such as adhesion on metal and glass, and on resin-coated metal (Sterman and Marsden, 1966).

When inorganic materials like glass fibers are reinforced with organic materials, interface region between organic and inorganic materials are involved in complex interplay of both chemical and physical factors. These factors include retention of product properties, adhesion, concentration gradients, coefficient of expansion and physical strength. The adhesion of the inorganic reinforcement is affected by the migration of water to polar surface. The bond between two dissimilar substances is destructed. By applying of silane coupling agent, a water resistant chemical bond is formed at the interface. Due to the special physical and chemical properties of silane coupling agent, the bond strength is increased and also de-bonding at interface is prevented (Krayden, 2009).

The general formula of silane coupling agent typically contains of two types of functional groups, as shown in Figure 1.2. In this study, (3-Mercaptopropyl)trimethoxysilane (MPTMS) was used as an adhesion promoter. The structural formula of MPTMS is shown in Figure 1.3. The X in silane coupling agent is a hydrolysable functional group such as amine, halogen, alkoxy and acyloxy. For MPTMS, the hydrolysable group present in the compound is methoxy group ($-OCH_3$). The alkoxy group (R-O) on silicon is hydrolyzed by the addition of water and silanol is formed. The hydrolysable functional group will then bond chemically on inorganic substrates through condensation. A stable siloxane bond (Si-O-Si) is formed between them and water is eliminated (Krayden, 2009). The overall bonding process is shown in Figure 1.4. The organofunctional group of MPTMS is a thiol group which is responsible to react with metal nanoparticles.
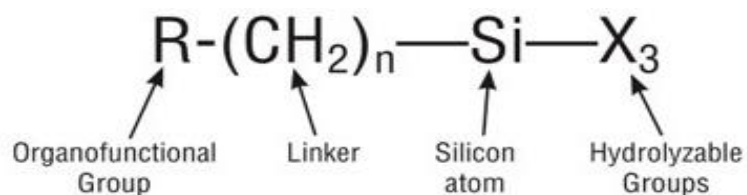
Figure 1.2: General formula of silane coupling agent (Gelest.com, 2018).
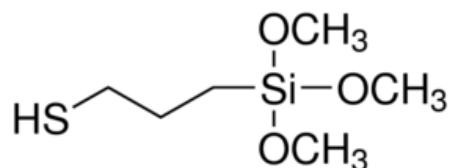
Figure 1.3: Structural formula of MPTMS.
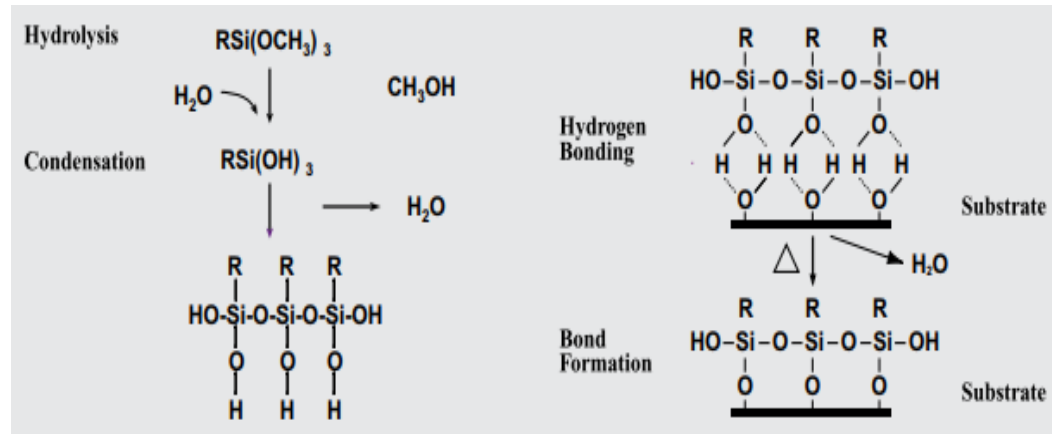
Figure 1.4: The overall bonding process of silane on inorganic substrate (Krayden, 2009).

1.4 Solar cell

Solar cell is also known as photovoltaic (PV) cell. It is a device that is made of semiconductor materials which is capable in capturing both solar energy from sunlight and non-solar energy like photons from incandescent bulbs, and then converting it into electricity by means of photovoltaic effect. Globally, the most common semiconductor material used in producing solar cell is silicon (Si). Silicon has the advantages of being environmental friendly and easily available in sufficiently large quantity because it is the second most abundance element found on earth crust (SolarServer, 2017).

Basically, two functions are required to be fulfilled by a photovoltaic device: photogeneration of charge carriers (holes and electrons) in light-absorbing material; and separation of charge carriers to conductive contact which is able to transmit electricity. Free electrons and holes will be formed at positive and negative junctions during sunlight absorption by solar cells. When DC electrical equipment is connected to p-n junctions of a solar cell, the current is transmitted to operate electrical devices.

Thousands of individual solar cells are connected electrically and fixed in a frame called module (solar panel). The larger modules are then grouped and form a solar array, as shown in Figure 1.5. Solar array functions as an electric power station center, converting solar energy into electrical energy and supply to residential users, industrial and commercial users.
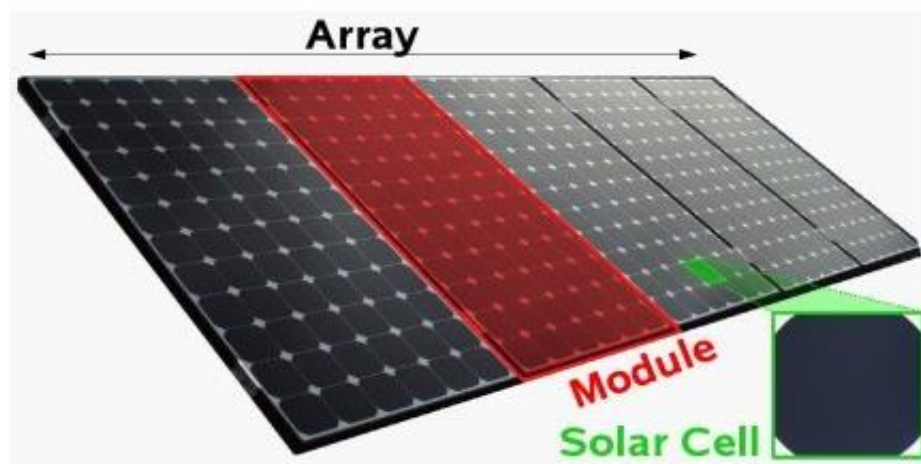
Figure 1.5: Schematic diagram of solar array (SolarGreen, 2019).

1.4.1   Solar cell design

The top layer of solar cell consists of a glass topmost layer, anti-reflective coating and metallic strips. The main function of the glass topmost layer is to protect the materials underneath it while anti-reflective coating maximizes the absorption of sunlight to reach the semiconductor and minimize the reflection of sunlight to the surrounding. The small grid pattern on solar panel is the grid of thin metallic strips below the glass (RGS, 2015).

The middle layer of solar cell consists of two layers of semiconductor and it is where the generation of electric energy takes place by means of photovoltaic effect. The upper layer is made out of n-type material (n-doped silicon), which is usually by mixing of silicon with a little amount of phosphorous. Thus, the silicon at this layer is negatively charged. On the other hand, the bottom layer is made of p-type material (p-doped silicon), which generally consist of silicon mixed with a little amount of boron and thus makes the silicon positively charged. Between these two layers, there is the p-n junction (RGS, 2015).

There are also two parts in the bottom layer of solar cell, namely rear metallic electrode and reflective layer. The rear metallic electrode is directly underneath the p-doped semiconductor. The rear electrode collaborates with the metallic strips in the top layer to generate electric current. The last layer is the reflective layer with

the purpose of reducing the loss of sunlight in the system. Different materials are used in different solar cells which depend on their application and cost (RGS, 2015).
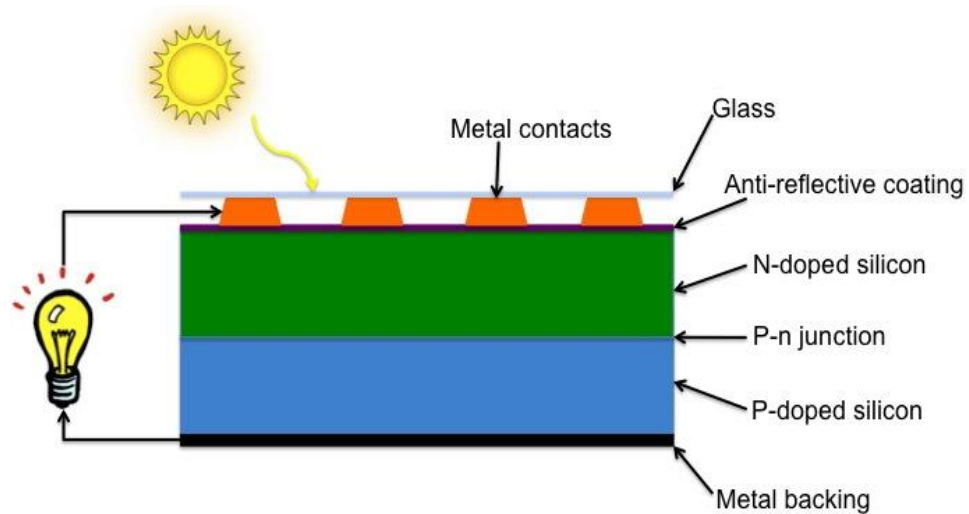
Figure 1.6: Schematic diagram of solar cell (RSG, 2015).

1.4.2 Working principle of solar cell

The working principle of solar cell is generally lies on the generation of electrons and holes between two different doped-semiconductors and the circulation of free electrons passing by a consumer and back to holes.

When sunlight strikes on the surface of a solar cell, charge carriers, holes and free electrons are generated. The semiconductor absorbs the light when the light reaches the middle layer. The junction creates internal field and some of the positive charges (holes) are separated from the negative charges (electrons). The light energy in the form of photons are absorbed and then the atom energy of the

13

semiconductors increases. The free electrons are swept into n-layer while the holes are swept into p-layer. Sometimes, the electrons fill the holes immediately at p-n junctions, without generating electricity. However, a barrier is formed quickly. The metallic strips on the top layer draw the electrons from n-doped layer. These free electrons are forced to move in one direction and thus an electric current is generated. The free electrons utilize the energy load to generate electricity when passing through the external circuit. After generating the electric current, the electrons move through the circuit until the rear electrode are reached. The electrons will then recombine with the positive holes in p-type material. The circuit is complete and current can be produced (RGS, 2015) (Leonics, 2017).

1.4.3   Type of solar cell

There are total of three major types of solar cell which are categorized according to the semiconductor materials used and the manufacturing technology: crystalline silicone PV module, amorphous silicon PV module and hybrid silicon PV module.

Crystalline silicone PV module can be further classified into two different types based on the type of crystalline silicon used: monocrystalline silicon (single) and polycrystalline silicon (multi). Both of the crystalline silicone PV modules have high conversion efficiencies at around 10-12%. However, as compared to polycrystalline silicon PV module, monocrystalline silicon PV module has higher conversion efficiency.

Amorphous silicon PV module is also known as thin-film silicon PV module, which has lower efficiency in the absorbing of light compares to crystalline silicon PV module. Thus, it is generally thinner in size. The typical power conversion efficiencies of amorphous silicon PV module is about 6%.

Hybrid silicon PV module is a combination of two types of silicon PV module, by enclosing the single crystalline silicon with thin layers of amorphous silicon. This kind of module is very sensitive toward indirect light and lower light levels. Among these three types of PV modules, hybrid silicon PV module has the highest conversion efficiency of around 17% (Leonics, 2017).
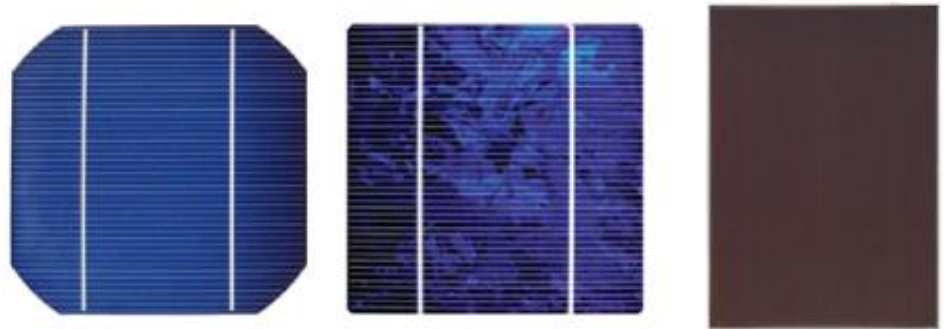
Figure 1.7: Types of solar cell: monocrystalline (left), polycrystalline (middle) and amorphous (right) silicon PV module (Hyder, 2019).

1.5 Dip coating

Dip coating method is employed for depositing a layer of material on a substrate by immersing and withdrawing the substrate into and from the reservoir solution. There are several factors that control the coated film structure and thickness: number of dipping cycle, temperature, pH value, solution composition and concentration, immersion time etc. By using dip coating method, a uniform and high quality films can be obtained, which is especially desirable in nanotechnology (Biolin Scientific, n.d.).

1.5.1 Self-assembly method

The nanoparticles films are deposited on substrate through dip coating technique via self-assembly method. According to Grzelczak, et al. (2010), self-assembly is defined as a process that nanoparticles or discrete components organize into ordered structure spontaneously. Self-assembly of nanoparticles has much interesting applications in nanotechnology. The chemical forces that organize self-assembly are strong covalent and ionic bonds; weak chemical interactions include hydrogen bond, van der Waals forces and hydrophobic-hydrophilic interactions. Self-assembly method can be utilized in the fabrication of several micro-complex and nanostructures. Self-assembly is applicable for any scale, not restricted to nanoscale only. Thus, it is known as a powerful bottom-up assembly method (Kajbafvala, et al., 2013).

When a substrate has been immersed in a solution containing activated stabilizer, a monolayer of solution components is formed spontaneously on the substrate through physisorption, by either covalent binding or electrostatic interactions. The common example of self-assembly method is the reaction of alkanethiols with a gold or silver surface (Biolin Scientific, n.d.).

1.6   Problem statement

In Malaysia, the electric energy is generated primarily by burning of limited fossil fuel sources such as fuel oil, coal and natural gas in power plants that bring large impacts and consequences to the surrounding environment. For example, greenhouse gases are produced during burning of fossil fuels which may lead to depletion of ozone layer and climate changes. The demand of electric energy in Malaysia has increased over the past decade because of development of economy. According to the data from Malaysia Energy Information Hub (MEIH), 134 billion kWh of electricity are generated and supplied to citizens of Malaysia in 2012 due to growth in populations (The Star, 2015). Fossil fuels are playing an important role in generating of electricity as they contribute the most to electric energy generation. However, due to over dependency, fossil fuels reserves are depleting rapidly as they are non-renewable resources (Samsudina, et al., 2016).

In recent years, solar energy has attracted the interest from society and it becomes a promising alternative resource to tackle the energy crisis, since it is a renewable resource. With the invention of several types of light harvesting devices like solar cell, solar energy can be captured and converted into electric energy. This kind of electricity generation method is more environmental friendly.

Nowadays, most of the solar cells available are made up of silicon which suffers an issue of low optical efficiency due to surface light reflection. Thus, the modification of the surface of solar cell becomes significantly important in order to generate a surface texture which is capable for light trapping into semiconductor materials and thus, increases light harvesting efficiency. One of the most effective ways to improve the light harvesting efficiency of solar cell is by incorporating of the metallic nanoparticles like silver metal on the surface of solar cell (Jeng, et al., 2015).

In this study, silver nanoparticles are synthesized through chemical reduction method with the presence of capping agent which will yield a high quality of particles in nanoscale. The silver nanoparticles are coated or deposited on the solar panel through dip coating or self-assembly process. In order to overcome the high photon energy from sunlight which is capable to break the bond at the interface and gives strong weathering resistance for outdoor purpose, a silane coupling agent is added as an additive to modify the surface of the glass substrate. Thus a strong and

stable adhesion is present between the surface of solar cell panel and silver nanoparticles.

1.7   Objectives

The objectives of this study are shown as below:

1. To synthesize silver nanoparticles using silver nitrate as the metal precursor, sodium borohydride as reducing agent and dodecanethiol as protecting agent through chemical reduction process.

2. To study the factors that will affect the formation of silver nanoparticles during chemical reduction process.

3. To characterize and study the surface morphology as well as particle sizes of the synthesized silver nanoparticles using UV/Vis spectrophotometry, X-ray diffraction (XRD) fourier-transform infrared spectroscopy (FTIR), Scanning Electron Microscopy (SEM), Atomic Force Microscopy (AFM) and light microscopy (LM).

4. To investigate the enhancement in light harvesting efficiency of solar cell which has been incorporated with silver nanoparticles by measuring the power output of solar cell.

1.8   Scopes of study and limitation

In this study, silver nanoparticles are synthesized using silver nitrate as the metal precursor, sodium borohydride as reducing agent and dodecanethiol as protecting agent through chemical reduction process. Ethanol is used as the synthesizing medium while toluene is used as the medium for re-dispersing of nanoparticles medium. In order to study the effect of concentration of reducing agent added, concentration of stabilizer and temperature on the particle size of the silver nanoparticles synthesized, different molar ratio of sodium borohydride and dodecanthiol (DDT) will be added to react with the metal precursor. At the same time, the synthesis process is carried out in both room temperature and in an ice bath.

Several characterization tests will be performed to determine the characteristic of synthesized silver nanoparticles, which include UV-Visible spectrophotometry (UV-Vis), scanning electron microscopy (SEM), atomic force microscopy (AFM), Fourier-transform infrared spectroscopy (FTIR) analysis, X-ray diffraction (XRD) and light microscopy (LM).

The silver nanoparticles synthesized are then coated on the solar cell through immersion or dip coating method. By applying the coupling agent, MPTMS, the metallic nanoparticles are self-assembled on the surface of solar cell. The concentration of coupling agent used will affect the size, number of layer and

distribution of metallic nanoparticles coated on substrate. The light harvesting efficiency of solar cell is then studied. Before coating of silver nanoparticles, the solar cell panels are immersed in different concentration of MPTMS at room temperature. The light harvesting efficiency of solar cell incorporated with silver nanoparticles and coupling agent is studied by measuring the power output of the solar cell.

There are some limitations in this study. Firstly, the effect of incorporating of silver nanoparticles on light harvesting efficiency is only performed on silicon type solar cell but not other type of photovoltaic cells. Thus, the outcome of this study may only valid for silicon type solar cell. Besides, the number of layer and distribution of silver nanoparticles coated on the surface of solar cell cannot be visualized, detected and measured without the use of high tech instruments, such as SEM and TEM. Thus, the correlation between the number of layer and distribution of deposited metallic nanoparticles and light harvesting efficiency of solar cell cannot be carried out easily in the course of the FYP.

CHAPTER 2

LITERATURE REVIEW

2.1 Synthesis of silver nanoparticles

Over the years, silver nanoparticles had received extensive attention and were studied widely by scientists. There are many synthesis methods that have been developed to synthesize silver nanoparticles. The main issue of concern when synthesizing silver nanoparticles is the controlling of the physical properties of nanoparticles, such as producing uniform size and shape of nanoparticles, identical structure and crystallinity, morphology and chemical composition. The synthesis methods of silver nanoparticles are categorized based on similar approaches or the differences such as top-down against bottom-up, conventional against nonconventional and also green against non-green synthesis methods (Güzel and Erdal, 2018).

The conventional synthesis method includes the using of organic reducers, borohydride, citrate and two-phase system during the synthesis process. However, a non-conventional synthesis method involves vacuum evaporation, radiocatalysis, laser ablation electrocondensation, and electrodeposition. On the other hand, utilizing of environmentally friendly agents like natural products during the synthesis process is considered as green synthetic method (Güzel and Erdal, 2018).

Generally, the synthesis methods are classified into three main types: chemical method, biological method, and physical method. Beyond that, there are several sub-methods that have been developed which are further differentiated under these three main types of synthesis methods. Each method has its own advantages in the synthesis of silver nanoparticles.

2.1.1 Chemical methods

Chemical methods are the techniques that utilize the chemical reagents to synthesize the metal nanoparticles in the presence of solvent. There are three important components that are usually employed in this approach: metal precursors or metal salt, reducing agent and stabilizer or capping agent. Two stages are involved in the reduction of metal salts, nucleation process and subsequent growth of nuclei. It has been reported that the size and shape of the synthesized silver nanoparticles depended on these two steps strongly (Natsukil, et al., 2015). Through adjustment of the reaction conditions such as reaction temperature, metal precursors, pH, reducing agent and capping agent, the initial nucleation and subsequent growth process of silver nanoparticles could be controlled and limited in order to obtain the silver nanoparticles in small size with a uniform spherical shape and narrow diameter distribution.

Chemical methods are more commonly used compared to physical and biological methods due to their advantages such as high yields, require of simple equipment, low preparation cost, ease of production, yield of nanoparticles without agglomeration, variety of size and shape are possible, mild reaction condition and shorter preparation time (Song, et al., 2008). However, the chemical reagents used as reducing agent, stabilizer and solvent might be hazardous, toxic and harmful to human and environment. Other than that, the synthesized nanoparticles might not be pure enough due to sedimentation of chemicals on particle surface (Zhang, et al., 2016).

Chemical reduction method was widely applied in the synthesis of silver nanoparticles using either organic or inorganic reducing agents such as sodium borohydride, sodium citrate, N, N-dimethylformamide (DMF), polyol process and Tollens reagent. These reducing agents are used to reduce silver ions, Ag^+ into silver, Ag^0 in non-aqueous or aqueous solutions. Subsequently, the metallic silver agglomerates into oligomeric clusters, followed by the formation of silver nanoparticles. A protective agent is important to be introduced during the synthesis process. It protects the nanoparticles from agglomeration through the interaction with particle surfaces. Different types of surfactant or stabilizer can be used as protective agent such as citrate, polyvinylpyrolidone (PVP), 1-dodecanthiol (DDT), polyvinyl alcohol (PVA) and sodium dodecyl sulfate (SDS).

According to Mavani and Shah, et al. (2013), silver nanoparticles with an average size of 20 nm were produced through reduction of silver nitrate by sodium borohydride in the presence of PVP as protecting agent. However, by using the same starting materials as mentioned with different stabilizer, DDT, silver nanoparticles with particle size of 4 nm were synthesized (Farrell, et al., 2013). In another report, polyoxometalates was used as both reducing agent and stabilizer to synthesize spherical shape silver nanoparticles with the diameter of 15.3 ± 3.4 nm (Troupis, et al., 2002). Moreover, polyol process was utilized in the preparation of monodisperse silver nano-cubes, by using ethylene glycol as reducing agent while PVP polymer as stabilizer. The particle size of silver nanoparticles with 20 nm was synthesized successfully (Saleh and Gupta, 2013).

Micro emulsion is a thermodynamically stable mixture of aqueous and organic phase that is stabilized by surfactant. It forms spontaneously at ambient temperature and consists of small droplets which possess of large interfacial area. Micro emulsion is categorized into three different types: oil-in-water (o/w), water-in-oil (w/o) and water dispersed in supercritical CO_2 (W/sc-CO_2). The initial spatial separation between metal salt and reducing agent in two immiscible solutions is the working principle for the synthesis of silver nanoparticles in a two phase system (Parveen, et al., 2016). According to Zhang, et al. (2007), silver nanoparticles with the size range of 2.5-15 nm were prepared through w/o micro emulsion between silver nitrate (metal precursor) and hydrazine hydrate (reducing agent) solubilized

in water while dodecane as oil phase with the presence of sodium bis(2-ethylhexyl) sulfosuccinate (AOT) as surfactant.

Electrochemical synthesis method was used to synthesize silver nanoparticles with controllable particle size by altering the electrolysis parameters and composition of electrolytic solutions. According to Johans (2002), polyphenylpyrrole coated silver nanospheroids with size range of 3-20 nm were prepared using electrochemical reduction method at liquid-liquid interface. In another study, 10-20 nm particle size of spherical silver nanoparticles were synthesized in aqueous solution via electrochemical reduction in the presence of poly N-vinylpyrrolidone as stabilizer (Ma, et al., 2004).

Microwave-assisted synthesis method can be utilized to produce silver nanoparticles with smaller size and high degree of crystallization. This method has the advantages of less energy usage, short reaction time, less chemical waste and better product yield without agglomeration. It has been reported that 12 nm particle size of silver nanoparticles were produced through microwave-assisted method by employing starch as reducing agent and template to prevent aggregation of the nanoparticles (Sreeram, et al., 2008).

2.1.2 Physical methods

Physical approaches are the techniques that are used for synthesizing silver nanoparticles with identical size and shape through the control of power, arc discharge and temperature. Other physical approaches that have been developed and reported by scientists and researchers are evaporation-condensation, thermal decomposition, ceramic heating process, arch discharge technique and laser ablation. These methods have their own pros and cons. One of the significant advantages is that these techniques are solvent free system which means that solvent contamination is absent in the preparation of thin films. In addition, the uniformity of nanoparticles distribution can be obtained through physical methods. However, the disadvantages of physical approaches are time consuming with high energy consumption (Alqad and Saleh, 2016).

According to Iravani, et al. (2014), metallic nanoparticles could be synthesized through physical approaches of evaporation-condensation method, which was carried out in a tube furnace at atmospheric pressure. A metal precursor was placed in the center of furnace and then it was then heated and vaporized into carrier gas. The evaporated vapor was then cooled down at an appropriate rate. High concentration of particles with nano-scale was formed. The generated nanoparticles were highly stable due to the consistency of temperature of the heater surface with time. With the increase of temperature of the heater surface, geometric mean diameter and total number concentration of nanoparticles would also increase.

Silver nanoparticles with the geometric mean diameter range of 6.2-21.5 nm were produced.

Laser ablation of metallic bulk materials in solution was utilized to synthesize silver nanoparticles. The advantage of this method is pure metallic colloid could be formed due to the absence of chemical reagents in solution and it is useful for further applications. By changing the laser pulses number, size of nanoparticles could be controlled. According to Tsuji, et al. (2003), silver nanospheroids with an average size of 20-50 nm were produced using laser ablation in water with femtosecond laser pulses at 800 nm. In addition, silver nanoparticles with narrow size distribution in water were synthesized through irradiation of silver materials source with 532 nm laser beam without adding of chemical additives (Pyatenko, et al., 2004)

On the other hand, silver nanoparticles with an average size 10 nm could be synthesized using thermal decomposition method through the complexation process between silver and oleate (Jung, et al., 2006). Thermal decomposition method involved the use of water as solvent, under moderate to high temperature and pressure condition. However, according to Tien, et al. (2008), arc discharge method was used to synthesize silver nanoparticles of 10 nm in size and concentration of approximately 11 ppm and 19 ppm. The silver metal was sputtered into reaction mixture by mean of physical deposition of silver into glycerol.

Moreover, according to Siegel, et al. (2012), round shape silver nanoparticles with the size of 3.5 nm were produced using the same method as mentioned above.

2.1.3 Biological methods

Biological methods are also known as green methods which are the techniques that utilize biomolecules and biological microorganisms such as plants extracts, polysaccharide, yeast, bacteria, fungi and algae, to act as reducing agent and also stabilizer. Biological methods are biocompatible and environmentally friendly approaches which use non-hazardous and non-toxic chemicals in the synthesis of metal nanoparticles. It is a low cost technique that provides a wide range of resources for the synthesis of the silver nanoparticles. However, large quantity of silver nanoparticles is hard to be obtained through biological synthetic technique (Zhang, et al., 2016).

Bacteria is potentially a bio-factory for synthesizing of silver nanoparticles for the production of both intra- and extracellularly inorganic materials. According to Suresh, et al. (2010), spherical silver nanoparticles with an average size less than 15 nm were synthesized through biosynthesis using a bacteria, *Shewanella oneidensis*, as reducing agent. In another reported method, the bacteria, *Bacillus sp.* was used to synthesize silver nanoparticles with a particle size of 20 nm (Fayaz, et al., 2010).

On the other hand, the natural products extracted from *Strychnos potatorum* leaves were utilized to produce silver nanoparticles by reducing silver nitrate. These nanoparticles had an average size of 28 nm with cubic and hexagonal structure (Kagithoju, et al., 2014). Moreover, silver ions were reduced to silver nanoparticles in the medium of *Aloe vera* extract without the addition of other chemical as reducing agent. The size of nanoparticles was found to be within the range of 70-192 nm. The particles size could be controlled through varying the conditions such as temperature and time of hydrothermal process (Tippayawat, et al., 2014). The nanoparticles which are synthesized through biological preparation show the bactericidal activity and they are very powerful against microbes.

2.2   Factors that affect the formation of silver nanoparticles

There are a few factors that might affect the formation of silver nanoparticles and their physical properties in term of particle size, degree of crystallinity, size distribution, particle shape and also the percentage yield. The physical properties of silver nanoparticles could be controlled by adjusting the reaction parameters during chemical reduction reaction and thus the nanoparticles with desired physical properties could be obtained.

2.2.1 Effect of initial metal precursor concentration

The concentration of silver metal precursor is one of the major parameters that will affect the synthesis of silver nanoparticles. This factor was investigated and studied by preparing different concentration of initial silver ions while the other parameters were kept constant in order to determine the suitable amount of silver ions for preparation of silver nanoparticles. During the chemical reduction of silver metal salt, the silver ions, Ag^+ from the metal salt will be reduced by a reducing agent to form silver Ag^0. The ionic chemical equation of this particular reduction reaction is shown below.

$$Ag^+ + e^- \longrightarrow Ag^0$$
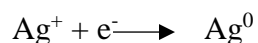
According to Song, et al. (2008), the sequence of the reagent addition was very important during the synthesis of silver nanoparticles through chemical reduction method. The silver metal salt (silver nitrate) solution should be added dropwise into reducing agent (sodium borohydride) solution with stabilizer. Thus, high stability of silver nanoparticles could be produced. However, the reverse sequence of reagent addition might be resulted in immediate precipitation of particles. In addition, the colour of the silver nanoparticles solution depends on the concentration of metal salt solutions. When the initial concentration of silver metal salt solution increases, the maximum plasmon peak intensity would increase and

the colour of the solution would turn from yellow to brown. This indicates the formation higher concentration of silver nanoparticles.
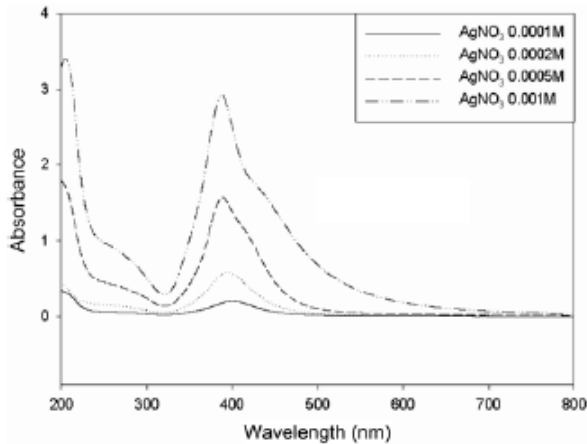
Figure 2.1: UV/Vis absorption spectrum of the AgNPs synthesized with different concentration of silver nitrate solution (Song, et al., 2008).

The rate at which LSPR would be achieved increases with the increasing of initial concentration. The formation of silver nanoparticles would give a plasmon peak between the wavelength ranges of 400-490 nm with an ideal bell shape spectrum due to the surface plasmon excitation effect (Dada, et al., 2018). On the other hand, when the plasmon peak became narrower, it indicates the existence of narrower range in size distribution (Anigoll, 2017).

2.2.2 Effect of reducing agent concentration

The concentration of reducing agent is another parameter that will affect the formation of silver nanoparticles. There are a lot of journal articles that reported the effect of reducing agent concentration during synthesis of silver nanoparticles through chemical reduction method. This factor was investigated and studied by varying the molar ratio of reducing agent to silver metal salt while the other parameters remained constant.

According to Song, et al. (2008), the higher the concentration of reducing agent, the higher the percentage yield of silver nanoparticles. This is because the reduction reaction is more complete as more silver metal salt could be reduced by the reducing agent and form more silver nanoparticles. Based on the UV/Vis spectrum, the information of degree dispersion of silver nanoparticles and their size distribution could be obtained. Based on the results reported, silver nanoparticles would aggregate when there was only small amount of reducing agent, such as sodium borohydride, added due to the reduction of electron density of particle surface. On the other hand, when the concentration of reducing agent increases, the intensity of maximum plasmon absorption peak of silver nanoparticles became higher and the width of absorption peak became narrower. This indicated that smaller silver nanoparticles with better degree of dispersion were produced. This is because the absorption of boron hydroxide to the surface of nanoparticles was avoided by thick BH_4^- layer. Thus, the nanoparticles were well dispersed (Song, et

al., 2008). However, according to Solomon, et al. (2007), an adequate amount of reducing agent should be added because too much of reducing agent would increase the overall ionic strength of nanoparticles. Thus, the particles would aggregate and bigger size of particles would form.
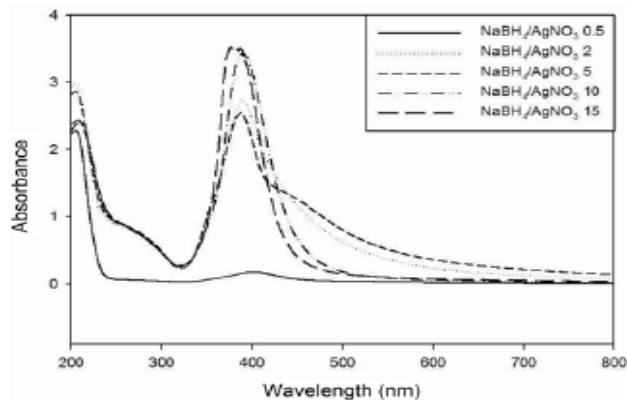
Figure 2.2: UV/Vis absorption spectrum of the AgNPs synthesized from different concentration of reducing agent (Song, et al., 2008).

2.2.3 Effect of stabilizer concentration

The purpose of adding the stabilizer or capping agent is to protect the nanoparticles from aggregation, agglomeration and growth through steric stabilization. When the concentration of stabilizer added increases, the plasmon absorption peak of silver nanoparticles becomes narrower and the intensity of the peak increases. The results obtained confirmed the nanocrystalline characteristic and proved that the silver nanoparticles were well dispersed. Meanwhile, the smaller size of nanoparticle was formed and the size distribution range was narrow due to the steric effect of nanoparticles (Song, et al., 2008).
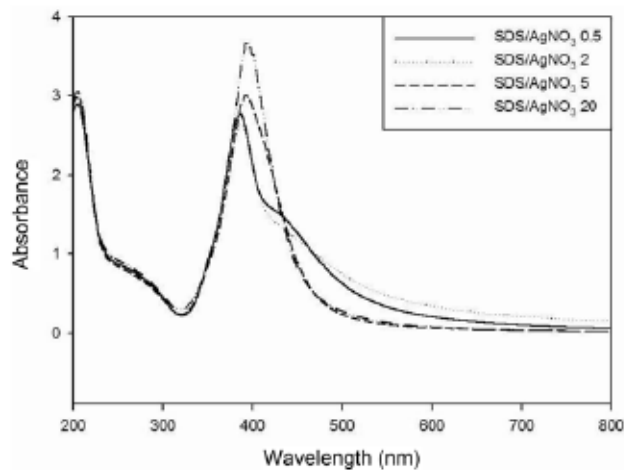
Figure 2.3: UV/Vis absorption peak of AgNPs synthesized with different concentration of stabilizer (Song, et al., 2008).

According to Farrell, et al. (2013), adequate amount of stabilizer should be added during the synthesis of silver nanoparticles in order to protect the nanoparticles from aggregation and agglomeration by absorbing to their surface. After reaching an optimum concentration, the particle size of nanoparticles would increase with the increasing of stabilizer concentration due to greater adsorption at water interface. More water interfacial area was stabilized (Lee, et al. 2017).

2.2.4 Effect of temperature

According to Jiang, et al. (2010), the higher the temperature, the bigger the size of particles. When the temperature increased from 17 ºC to 32 ºC, the size of triangular shape of silver nanoparticles increased from 90 nm to 180 nm. Similar trend was observed for sphere shape nanoparticles. The spherical shape of silver nanoparticles

growth from 25 to 48 nm with the increase of temperature from 17 ºC to 32 ºC. The silver nanoparticles were found to be formed at the early stages, nucleation and subsequent growth process. At high temperature, the rate of reaction was higher and the nucleation and growth process of silver nanoparticles were fastened. Thus the synthesized nanoparticles growth larger in size. Meanwhile, it might be also resulted by the fusion growth process.

2.2.5   Effect of pH

Table 2.1: The size of AgNPs corresponding to pH (Alqadi, et al., 2014)

pH $\pm$ 0.01	The peak absorption (arb.u.)	The wavelength (nm) $\pm$ 0.3	The size of AgNPs (nm)
7.00	1.193	428.0	74.00 ± 3.11
8.00	1.955	418.5	67.00 ± 1.59
8.50	2.197	416.0	57.00 ± 1.37
9.00	2.287	410.5	54.00 ± 1.95
10.00	2.476	404.0	43.00 ± 1.87
11.00	2.716	397.0	32.00 ± 1.55

The formation of silver nanoparticles was more favorable in alkali condition. When the pH of the reaction medium increased, the absorbance of the plasmon absorption peak increased which indicated that the size of synthesized nanoparticles decreased (Alqadi, et al., 2014).

2.3 Solar cell efficiency

Throughout the years, there are several challenges and issues that have been encountered in the manufacturing of solar cell which include the processing cost and light harvesting efficiency. Thin film solar cell is a good replacement for production cost reduction, however it has lower light harvesting efficiency which might be due to not-uniformly-distributed crystalline structure of silicon. Amorphous silicon solar cell has the lowest efficiency of about 12%, follows by polycrystalline silicon solar cell with efficiency of around 17%, and monocrystalline silicon solar cell shows the greatest efficiency within the range of 25-30%. The absence and presence of grain boundaries in crystalline silicon solar cells affect the flow of excited electrons where the former does not have any boundaries to obstruct the movement of excited electrons while the latter inhibits the continuous flow of electrons. Thus, the efficiency of the solar cell drops dramatically to about 10-15%. There are a lot of research studies that have been carried out to improve the light harvesting efficiency of solar cell.

In the study reported by Jeng, et al. (2015), gold and silver nanoparticles were incorporated on both multicrystalline silicon (mc-Si) and copper-indium-galium-diselenide (CIGS) though spin-coating method in order to investigate and study the enhancement of light harvesting efficiency of solar cell. For mc-Si solar cell, suitable concentration of gold and silver nanoparticles deposited on the surface of solar cell had improved the light harvesting efficiency by 5.6% and 4.8%

respectively. On the other hand, the coating of gold and silver nanoparticles on the surface of CIGS solar cell at suitable concentration resulted in an improvement of light harvesting efficiency of 1.2% and 1.4% respectively.

In another study, the poly(methyl methacrylate-co-acrylic acid) (P(MMA-co-AA)) nano-spheres with the average diameter size of 101 nm were incorporated on the surface of solar cell. This surface modification had improved the light harvesting efficiency of solar cell to about 1.6 times better than a bare solar cell (Lee, et al., 2017). Moreover, the light harvesting efficiency of solar cell was further improved by 2.8 times as Ag-incorporated P(MMA-*co*-AA) nano-spheres were deposited on the surface of solar cell. The deposited silver nanoparticles functioned to scatter more light into the active layer of solar cell and thus more free carriers were generated.

According to Mizuno, et al. (2012), silver nanoparticles were coated inside the rear ZnO:Ga layer of thin film hydrogenated microcrystalline Si (μc-Si:H) solar cell through self-assembly wet-chemical method. The light trapping effect was enhanced about 75% in current density with the optimization of two important parameters, surface coverage and location of silver nanoparticles in the ZnO:Ga layer.

The effect of the incorporation of silver nanoparticles on light harvesting efficiency of thin film solar cell was also investigated by Phillai, et al. (2007) who found that there was a significant light absorption enhancement as the wavelength of silver nanoparticles near to the band gap of Si. A sevenfold enhancement was observed for wafer-based thin film solar cell and 16-fold enhancement for thin-silicon-on-insulator (SOI).

Other than that, a few other journal articles also reported that the light harvesting efficiency of solar cell could be enhanced through self-assembly of AgNPs on the surface of solar cell. According to the research work done by Zi, et al. (2016), silver nanoparticles with an average size of 320 nm were incorporated on the surface of thin film silicon solar cell which had enhanced the back reflector and light harvesting efficiency of about 19.5%. However, when the optimized size of silver nanoparticles, 35.2 nm, were coated on solar cell, it resulted in an enhancement of light trapping efficiency of more than 70%. On the other hand, silver nanoparticles with an average size of 30 nm were employed to modify the solar cell surface through evaporation and condensation coating method and increased the conversion efficiency of solar cell within the range of 6.195% to 6.696% (Jung, 2013).

2.4   Factors that affect the light harvesting efficiency of solar cell when silver nanoparticles are coated on its surface

Due to the plasmon enhancement and backscattering effect of silver nanoparticles, the reflectance of the solar cell could be reduced and light harvesting efficiency could be improved by incorporating silver nanoparticles on its surface. The physical properties of the silver nanoparticles which are coated on the surface of the solar cell, such as particle size, shape, particle density and surface coverage will influent their localized surface plasmon resonance characteristic and backscattering effect. Besides that, the surface reflectance of solar cell is influenced and thus the light trapping efficiency of solar cell are affected.

2.4.1   Effect of particle size

In the study of Dai, et al. (2012), silver nanoparticles with different sizes, 68nm and 85 nm, were coated on the surface of silicon by sputter-anneal process. It showed that the excited wavelengths of silver nanoparticles with 68 nm and 85 nm in size were 380 nm and 420 nm respectively. When the size of metallic nanoparticles increased, there would be a red-shifting of the nanoparticles wavelength which is resulted by a larger relaxation time of electrons. The solar cell reflectance for silver nanoparticles with larger size was much lower than smaller particle size due to the higher order modes of bigger size of nanoparticles which scatter more light into solar cell. However, if the silver nanoparticle size was too large, the light harvesting

efficiency would be decreased by means of reducing in the scattering cross section of nanoparticles. Therefore, an optimum size of silver nanoparticles is required in order to obtain higher order modes and scattering cross section.

2.4.2 Effect of particle shape

The particle shape is one of the significant factors that will also affect the surface reflectance and light trapping efficiency of solar cell. The irregular shape of silver nanoparticles have a higher reflectance effect. However, the reflectance effect decreases at a certain wavelength. This is because the irregular shape of silver nanoparticles acts as a homogeneous layer that will slightly reduce the surface reflectance (Dai, et al., 2012). Thus, a uniform and regular spherical shape of silver nanoparticles is better than irregular shapes in term of light harvesting efficiency.

2.4.3 Effect of particle density and surface coverage

According to the study reported by Dai, et al. (2012), surface reflectance decreases when silver particle density and surface coverage increase. As the silver nanoparticle density and the surface coverage of nanoparticles on solar cell decrease, the phenomenon of quadrupolar mode resonance of silver nanoparticles would occur. This phenomenon would occur when only the surface of silicon was not completely covered by scattering cross section of metallic nanoparticles. Scattering cross section of silver nanoparticles corresponds to the incident light

frequency. When there was low particles density, the incident light frequency was further apart from quadrupolar mode resonance position, thus the surface reflectance increases.

2.5   Coupling agent

The main purpose of adding the coupling agent is to improve the binding of organic materials on inorganic substrate by forming a strong chemical bond (coupling). The coupling agent acts as an adhesion promoter. It was found that the plasmon resonance of nanoparticles would be shifted and broaden when the adhesion layer was weakened (Gothe, et al., 2018). There are various types of coupling agents available, but (3-mercaptopropyl)trimethoxysilane (MPTMS) with the presence of two functional groups at both terminals of the molecule is the best coupling agent for improving the adhesion strength of nanoparticles on the surface of a substrate. This is because it will form mono-dielectric adhesion layer which is able to prevent the shift in plasmon resonance of metallic nanoparticles.

According to Pilipavicius, et al. (2015), MPTMS had higher total surface free energy and good wetting properties compared to other silane coupling agent. When the silane coupling agent, N-[3-(Trimethoxysilyl)propyl]ethylenediamine (AEAPTMS) was used in the coating of silver nanoparticles on a substrate, large amount of primary and secondary amine groups present in the molecule would induce stronger attraction and resulted in aggregation of silver nanoparticles.

However, this situation was not observed in the incorporation of silver nanoparticles using MPTMS.

CHAPTER 3

MATERIALS AND METHODS

3.1   Chemicals

In this project, chemical reduction method was used to synthesize the silver nanoparticles (AgNPs). Chemical reduction method was carried out by using a reducing agent, sodium borohydride ($NaBH_4$) to reduce a silver metal salt, silver nitrate ($AgNO_3$) in the presence of suitable capping agent or stabilizer, 1-dodecanthiol (DDT) in order to control the particle size by slowing down the nucleation process and limiting the growth of metallic particles through agglomeration (Nersisyan et al., 2003). The synthesized AgNPs were characterized and the morphology of metal nanoparticles was studied. Subsequently, the silver nanoparticles were coated on the glass surface of solar cell through immersion coating method with the application of a coupling agent, 3-(trimethoxysilyl)-1-propanethiol (MPTMS). Table 3.1 shows the chemical reagents used for the synthesis of AgNPs, while Table 3.2 shows the chemical reagents used in solar cell coating. AgNPs which were synthesized earlier were used as the metal nanoparticle precursor during coating of solar cell. Meanwhile, Table 3.3 shows the chemical reagents used for cleaning the solar cell before coating.

Table 3.1: Chemical reagents used for the synthesis of AgNPs

Chemical	Function	Producer
Silver nitrate	Metal precursor	Systerm®
Sodium borohydride (NaBH₄)	Reducing agent	Alfa Aesar
1-Dodecanethiol (DDT)	Stabilizer	Sigma-Aldrich
Ethanol	Reaction medium	HmbG® Chemicals
Toluene	Organic solvent	Chem Sola

Table 3.2: Chemical reagents used in solar cell coating

Chemical	Function	Producer
3-(Trimethoxysilyl)-1-propanethiol (MPTMS)	Coupling agent	Merck
AgNPs	Metal nanoparticle precursor	-
Toluene	Organic solvent	Chem Sola

Table 3.3: Chemical reagents used for the cleaning of solar cell and glass substrate

Chemical	Function	Producer
Hydrogen peroxide	Oxidizing agent	Systerm®
30 % Ammonia solution	Reducing agent	R&M Chemicals

3.2 Procedure

To study on the improvement of the light harvesting efficiency of solar cell by coating the silver nanoparticles with coupling agent, the procedures of this project were performed in three major parts, they are: (1) synthesis of AgNPs through chemical reduction method, (2) coating of solar cell with AgNPs and coupling agent via immersion coating method, and (3) testing on light harvesting efficiency of solar cell.

3.2.1 Synthesis of AgNPs via chemical reduction method

Chemical reduction method was performed to synthesize AgNPs. The chemicals required for this process is shown in Table 3.1. The stock solutions were prepared in 50 mL volumetric flask. 0.170 g of silver nitrate (0.02 M) and 0.681 g of sodium borohydride (0.36 M) were first dissolved separately in 50 mL ethanol through sonication. Different amount of sodium borohydride solution was added into five beakers according to $\frac{[\text{Sodium borohydride}]}{[\text{Silver nitrate}]}$ molar ratios, denoted as R, which is shown in Table 3.4. The stabilizer, 1-dodecanethiol was then added into each of the beakers which containing $NaBH_4$ solution at $\frac{1-Dodecanthiol}{[Silver\ nitrate]}$ molar ratios, denoted as S, of 2.60, 5.30, 10.6 and 15.9, for a total of four sets, as shown in Table 3.5. The solutions were mixed well using magnetic stirrer. 9 mL of the $AgNO_3$ solution was added dropwise into each of the beakers. The mixtures were stirred for one hour. To recover the AgNPs, the solutions were centrifuged at 7000 rpm for 20 minutes.

The supernatant was discarded and replaced with fresh ethanol. This step was repeated three times in order to remove the impurities and unreacted starting materials. 20 mL toluene was then added to AgNPs and the suspensions were sonicated in order to re-disperse the nanoparticles. The solution was transferred into a sample vial. The procedures for the synthesis of AgNPs were repeated in ice bath instead of at room temperature.

Table 3.4: The amount of NaBH$_4$ added into each beaker

R value	6	9	12	15	18
Concentration of AgNO$_3$ (M)	0.02	0.02	0.02	0.02	0.02
Concentration of NaBH$_4$ (M)	0.12	0.18	0.24	0.30	0.36

Table 3.5: The amount of DDT added into each beaker

S value	2.60	5.30	10.6	15.9
Concentration of AgNO$_3$ (M)	0.02	0.02	0.02	0.02
Concentration of DDT (M)	0.052	0.106	0.212	0.318

3.2.2   Surface treatment of glass substrate and solar cell

The glass substrate and solar cell were cleaned with distilled water under ultra-sonication for about 15 minutes. This process was repeated by using fresh distilled water. The piranha solution was prepared by mixing distilled water, 30 % ammonia solution and hydrogen peroxide, with the composition ratio of 5:1:1. The mixture was heated to 67 $^{\circ}$C. The glass substrate and solar cell were immersed into the piranha solution for 30 minutes in order to hydrophilize their surface. The treated solar cell and glass substrate were then rinsed with distilled water and dried in a vacuum oven at 60 $^{\circ}$C.

3.2.3   Immersion coating of glass substrate and solar cell

MPTMS solution with different concentration, 0.051 M, 0.153 M 0.256 M, 0.358 M, 0.460 M, 0.563 M, 0.665 M and 0.767 M were prepared in 100 mL of toluene. The solutions were stirred using glass rod to homogenize the mixture solutions. The treated solar cell and glass substrate were immersed in the MPTMS solution for 45 minutes at room temperature, 25 $^{\circ}$C. The coated solar cell and glass substrate were cured in a vacuum oven for 45 minutes at 60 $^{\circ}$C. The synthesized AgNPs solution was sonicated and diluted with 100 mL of toluene, with the dilution factor of 10. The solar cell and glass substrate were then immersed into the AgNPs solution for 45 minutes and then cured in a vacuum oven for another 45 minutes at 60 $^{\circ}$C.

3.2.4 Power output measurement of solar cell
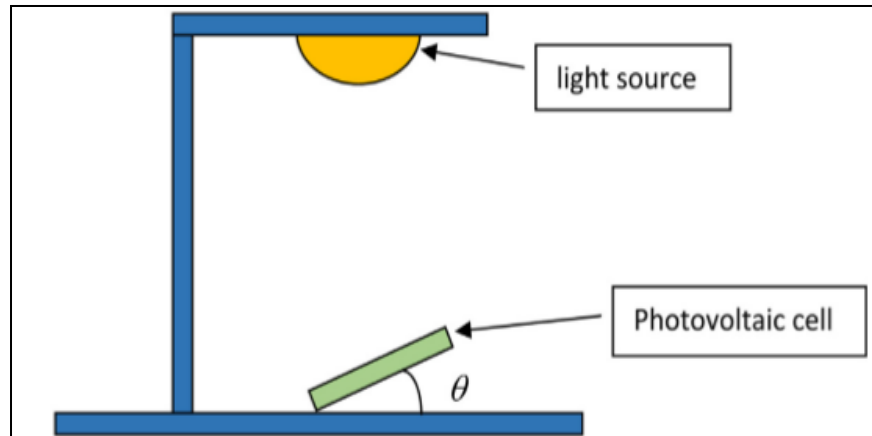
Figure 3.1: A diagrammatic representation of experimental setup for solar cell power output measurement (Lee et al., 2017).

The voltage and current of the solar cell before and after coating of AgNPs were measured under a white fluorescent lamp with the wavelength range between 400 nm to 800 nm using multimeter. In order to make sure all the measurements are done consistently, the distance between the light source and solar cell was fixed at 5 cm and the solar cell was fixed at an angle perpendicular to the light source. The setup of the apparatus is shown as Figure 3.1. Each of the samples was measured three times in order to get an average value. By using the current and voltage readings obtained, the power output of the solar cell was calculated using the formula below:

$$Power\ (mW) = current(mA) \times Voltage(V)$$

Meanwhile, the power output of the bare solar cell as well as the solar cell coated with AgNPs, were measured using an advanced instrument, DC Electronic Load UV Tester. For this instrument, a halogen lamp was used as the light source.

3.2.5 Determination of the concentration of Ag

The diluted AgNPs solution which has been used in the immersion coating process of the solar cell was sonicated to make sure the nanoparticles were re-dispersed completely in the toluene solvent. 10 mL of the solution was taken out and poured into a petri dish with pre-measured weight. The solvent was evaporated and the Ag solid was dried in the oven. The mass of the Ag solid obtained was weighed. By determining the mole of the Ag solid, the concentration of the Ag was calculated using the equation shown at below:

$$mole = \frac{mass}{molar\ mass} = Molarity\ x\ liters$$

3.3 Characterization

The synthesized AgNPs was characterized using UV-Visible spectrophotometry (UV-Vis), scanning electron microscopy (SEM), atomic force microscopy (AFM), Fourier-transform infrared spectroscopy (FTIR) analysis, X-ray diffraction (XRD) and light microscope (LM).

3.3.1 UV-Visible spectrophotometry (UV-Vis)

UV-Vis spectrophotometry is one of the methods used to confirm the formation of Ag particles and determine the plasmonic peak of synthesized AgNPs. The synthesized AgNPs solution was sonicated first in order to make sure the nanoparticles were re-dispersed well in the solution. Then, the solution was diluted using 10 mL of toluene with the dilution factor of 10 and subjected to UV-Vis scanning from 285 nm to 600 nm. The UV/Vis spectrophotometry spectrum was obtained.

3.3.2 Scanning electron microscopy (SEM)

SEM is an instrument used in the study of surface topography and composition of a substance. By coating on the treated glass substrate, the synthesized AgNPs was characterized using SEM in order to study the surface morphology of the nanoparticles. At the same time, the size and shape of the particles were determined with the SEM images obtained. Top view of the SEM images with the magnification power of 10000, 20000 and 50000 times were captured and studied.

3.3.3   X-ray diffraction (XRD)

XRD was used in this project in order to confirm the formation of the Ag particles and to determine the crystallinity of Ag particles. The Ag suspension which has been dried and ground into powder form was scanned continuously in the range of 10° to 80°, 0.60 second time constant at a scan rate of 2.0^o min^{-1}. XRD diffraction pattern was obtained with Cu $K\alpha$ radiation at 40 kV and 30 mA.

3.3.4   Atomic force microscopy (AFM)

AFM was another instrument used to characterize and study the surface morphology of AgNPs in this project. The 3-dimensional AFM image provides the information about the particle size, particle shape, and distribution of particle on glass substrate. Images captured by AFM give a clear magnified images of the surface of objects scanned. At the same time, the range particle size of the AgNPs coated on glass substrate was obtained via the application of computer software program.

3.3.5 Attenuated total reflectance (ATR) and Fourier-transform infrared spectroscopy (FTIR)

ATR and FTIR instruments were used in this project to confirm the formation of the Ag particles and to determine the presence of impurities in the compound, such as unreacted starting materials and stabilizer. At the same time, these instruments were also used to confirm that the stabilizer used, 1-dodecanethiol, was attached to the nanoparticles which is to prevent the coagulation and aggregation of particles, and maintain the particle size in nano-scale. The Ag solution was dried in an oven in order to completely remove the moisture and solvent. This is because the presence of the solvent and moisture might interfere and affect the peaks in the spectrum due to the high sensitivity of the instruments to moisture and water molecule. The Ag solid obtained was then ground into powder form. The Ag powder and 1-dodecanthiol solution were subjected to FTIR and ATR analysis in the range between 4000 cm^{-1} and 400 cm^{-1}.

3.3.6 Light microscope (LM)

The LM is an instrument that utilizes visible light and amplifying lenses to inspect tiny particles which are not able to be observed using naked eyes (Saladin and Miller, n.d.). LM is a useful tool in the study of surface morphology as it is able to produce a clear magnified image in a short time. The glass substrates which have been coated with coupling agent and AgNPs were observed under LM in order to obtain the information about the distribution of AgNPs on glass substrates. Images with the magnification power of 400 times were captured and studied.

CHAPTER 4

RESULTS AND DISCUSSION

4.1   UV/Vis spectroscopy

Different types of noble metal nanoparticles exhibit their localized surface plasmon resonance (LSPR) effect at different wavelength. For instance, silver nanoparticles scatter light strongly at the wavelength of 410 nm. However, the LSPR effect of the noble metal nanoparticles is highly dependent on their particle size and shape. An increase in the particles size and also sharpness or edges in the non-spherical shape of nanoparticles will cause a red shift in absorption spectra due to the high efficiency in charge separation. On the other hand, a decrease in the particle size will cause a blue shift in absorption spectra. A more symmetrical structure of the nanoparticles will enhance the LSPR intensity (Petryayeva and Krull, 2011).

According to Petryayeva and Krull (2011), the number of resonance absorption peak is determined by the number of modes the structure can be polarized by the incident light source. For example, the spherical shape of nanoparticles will have only one absorption peak while the non-spherical shape of nanoparticles will usually have more than one resonance absorption peaks, depends on its structure. The statement is illustrated in Figure 4.1. Moreover, different size and shape of nanoparticles will give a plasmon peak at different wavelength. For example, the

spherical shape of silver nanoparticles with an average size of 40-90 nm will give

a plasmon peak at the range of 400-480 nm due to LSPR effect.
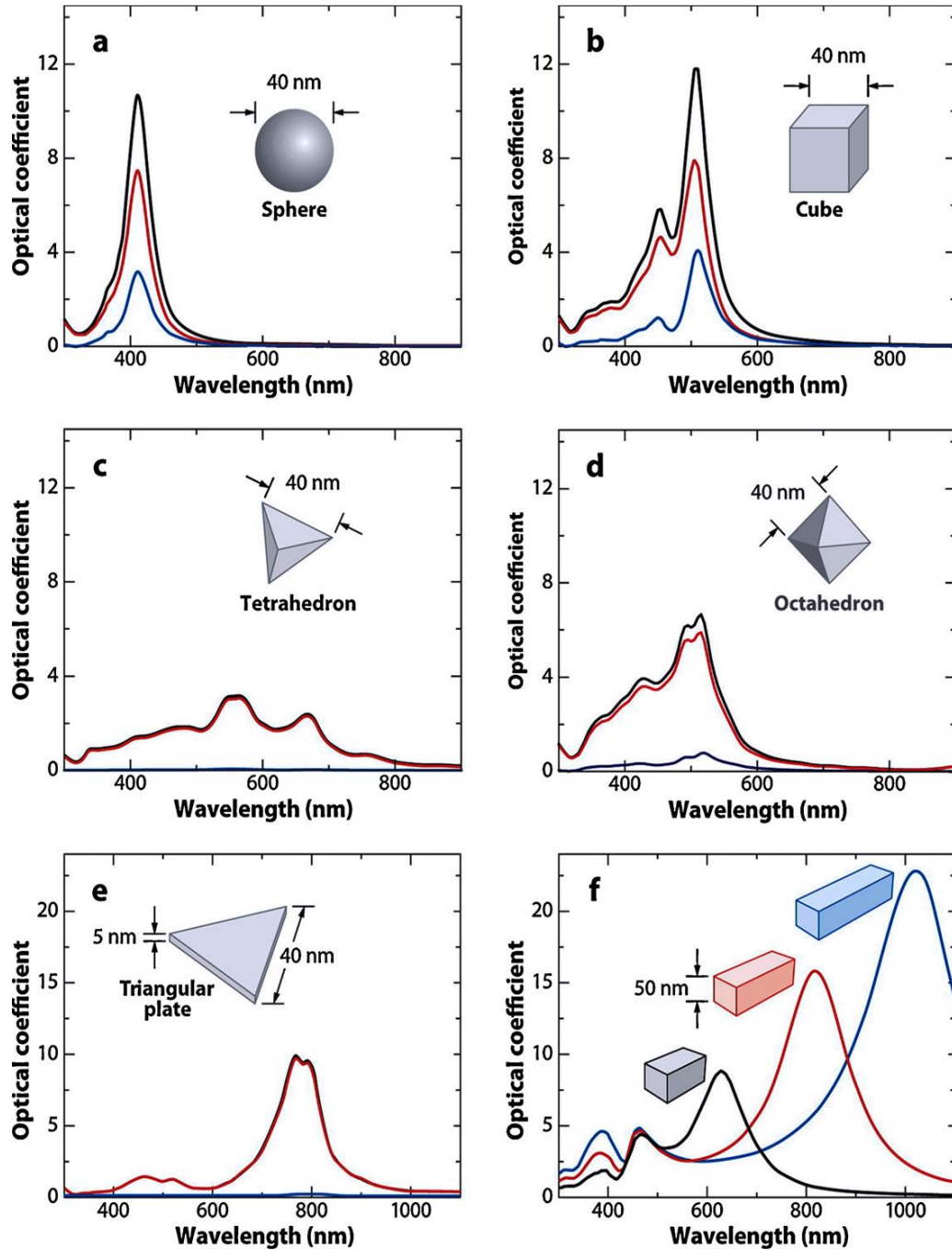
Figure 4.1: Number of resonance absorption peak of silver nanoparticles with different shapes and structure (Petryayeva and Krull, 2011).

By using the information obtained from the UV/Vis spectroscopy, the band gap energy of the silver nanoparticles could be determined. Band gap energy, E_{bg} is the energy that required to excite the electrons from the valance band to conduction band. The band gap energy of silver nanoparticles is slightly different when their particle size is difference. This is because smaller size of nanoparticles will give a blue shift effect (decrease in wavelength but increase in energy), while larger size of nanoparticles will give a red shift effect (increase in wavelength but decrease in energy). Wavelength shifting effect will affect the calculated value of band gap energy. According to Fredrick and Mangaka (2017), the silver nanoparticles have a theoretical band gap energy of 3.04 eV.

Band gap energy of silver nanoparticles is able to be calculated directly from UV/Vis absorption spectrum using Einstein's photon energy equation as shown at below:

$$E_{bg} = \frac{hc}{\lambda_{max}}$$

where λ_{max} is the maximum absorbance wavelength, h is the Planck constant and c is the speed of light (Gharibshahi, et al., 2017).

The synthesized silver nanoparticles solutions which had been re-dispersed in toluene were sonicated. The silver nanoparticles solutions were diluted using toluene with the dilution factor of 10. The diluted solution were then subjected to UV/Vis analysis with the scanning range of 285-600 nm.

4.1.1 Effect of concentration of reducing agent

The concentration of reducing agent, sodium borohydride ($NaBH_4$) will affect the particle size of silver nanoparticles synthesized. The effect of concentration of reducing agent on the size of synthesized metallic nanoparticles was studied and investigated by preparing the silver nanoparticles with various concentration of sodium borohydride while the other reaction parameters such as initial concentration of silver nitrate, concentration of capping agent and temperature were fixed at 0.02 M, 0.052 M and 0 °C respectively.

Figure 4.2 shows UV/Vis spectrum of silver nanoparticles solutions which were synthesized with different concentration of reducing agent, 0.24 M (R = 12), 0.30 M (R = 15) and 0.36 M (R = 18). The information obtained from the UV/Vis spectra were summarized in Table 4.1. Meanwhile, the band gap energy, E_{bg} of silver nanoparticles were calculated and tabulated in Table 4.1. From the spectrum obtained, it can be seen that the silver nanoparticles will give a plasmon peak at the range of 435-455 nm which falls in the given theoretical range 415-465 nm. Based on the plasmon peaks obtained, it proved that the silver nanoparticles were synthesized successfully.
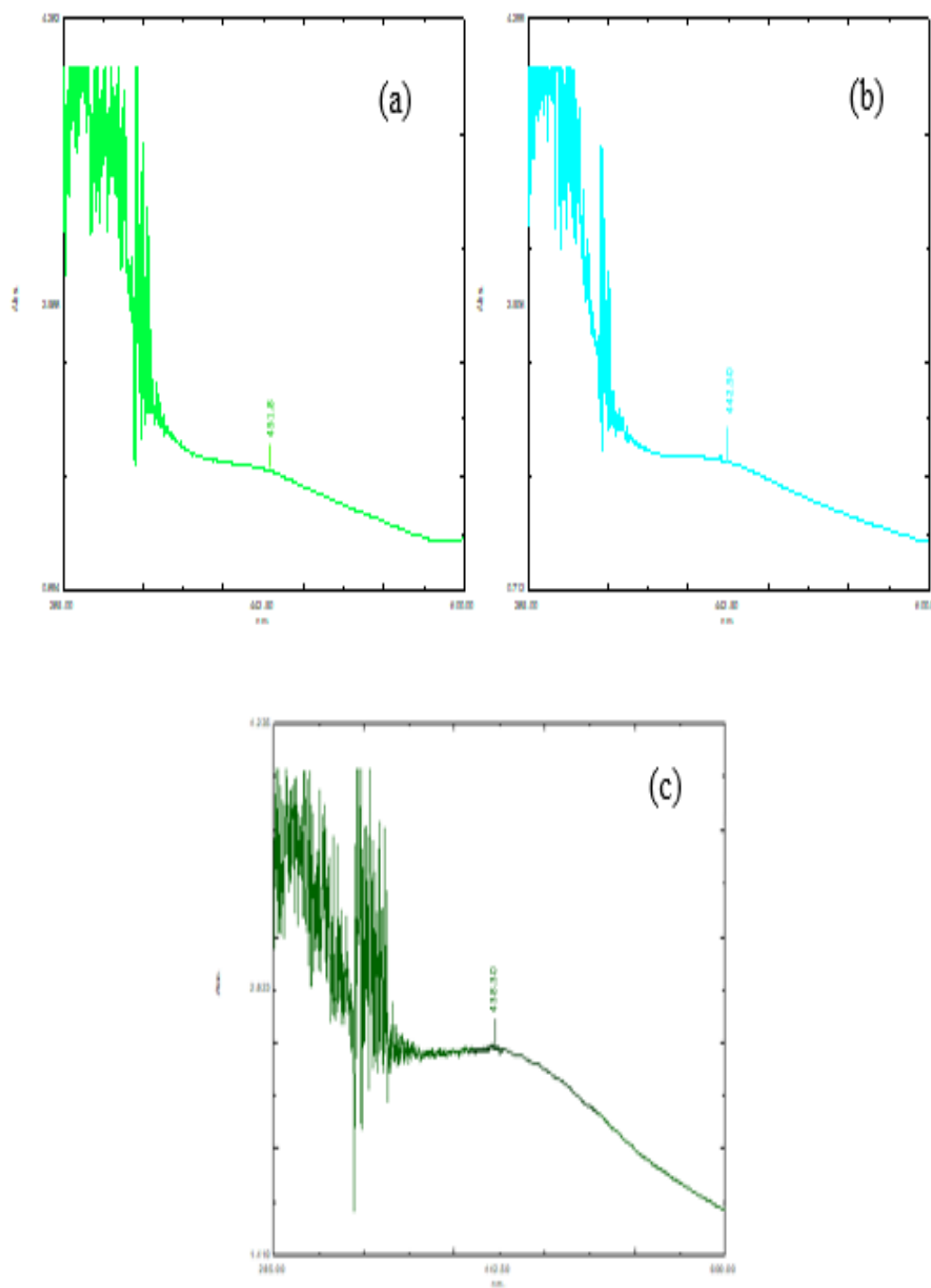
Figure 4.2: UV/Vis spectrum of silver nanoparticles solutions which were synthesized with different concentration of reducing agent, (a) 0.24 M (b) 0.30 M (c) 0.36 M.

Table 4.1: Absorbance and wavelength obtained from UV/Vis spectrum of silver nanoparticles solutions corresponding to R value with calculated E_{bg}

R value	Concentration of NaBH$_4$ (M)	Absorbance	Wavelength (nm)	E_{bg} (eV)
12	0.24	1.5492	451.80	2.75
15	0.30	1.6469	442.50	2.81
18	0.36	2.4556	438.30	2.83

On the other hand, it also shows that with increasing concentration of reducing agent from 0.24 M to 0.36 M, the absorbance of the plasmon peaks showed in the spectrum increases from 1.5492 to 2.4556. According to Mie theory, the results obtained indicate that smaller size of silver nanoparticles have been produced as the measured absorbance increases. Mie theory describes the absorption and scattering of electromagnetic plane wave by a homogeneous isotropic particles with spherical shape. It suggests the situations where scattering particles size is comparable to the light wavelength, rather than much smaller or larger (Acharya, 2017). According to Mie scattering theory, the smaller particles will scatter more light and more incident light will be absorbed by the particles. Thus, smaller the size of particles, higher measured absorbance will be obtained.

Other than absorbance, the calculated band gap energy, E_{bg} is also able to prove that the higher the concentration of reducing agent, the smaller the nanoparticles size. An increment in band gap energy and decrement in wavelength of the absorption peak of nanoparticles is a phenomena known as blue shift. According to quantum confinement theory, the blue shift phenomena occurs which is associated with decrease in size of nanoparticles. The holes and electrons are less confined by the potential barriers of the surface. Thus, the spacing of the electronic level and band gap energy increases with decreasing of particle size (Singh, et al., 2018). From the Table 4.1, it can be seen that with increasing of R value from 12 to 18, the wavelength of the absorption peak shifted from 451.80 nm to 438.30 nm, while the calculated E_{bg} increases from 2.75 eV to 2.83 eV. This indicated that the smallest size of silver nanoparticles were produced with highest concentration of reducing agent, R value of 18.

The results obtained in the study match to the theory stated by Song, et al. (2018), the silver nanoparticles with smaller size could be synthesized with increasing of concentration of reducing agent, sodium borohydride (NaBH$_4$). The ionic equation of reduction of silver nitrate by sodium borohydride is shown.

$$Ag^+ + BH_4^- + 3\ H_2O \longrightarrow Ag^0 + B(OH)_3 + 3.5\ H_2$$

When a small amount of sodium borohydride is added, the silver nanoparticles would aggregate and agglomerate. This is because the boron hydroxide which is produced through hydrolysis of sodium hydroxide will attach to the surface of nanoparticles. Lower concentration of BH_4^- will result in the reduction of surface electron density. However, when the excess amount of sodium borohydride is added, the silver nanoparticles could be maintained in smaller size due to the electrostatic stabilization as the particles were surrounded by thick BH_4^- ion layer. The thick BH_4^- ion layer prevents the absorption of boron hydroxide, $B(OH)_3$ to the surface of nanoparticles. Thus, the silver nanoparticles were well-dispersed in the solvent. In this case, sodium borohydride not only acts as a reducing agent, but also serves as a capping agent to protect the nanoparticles from agglomeration.
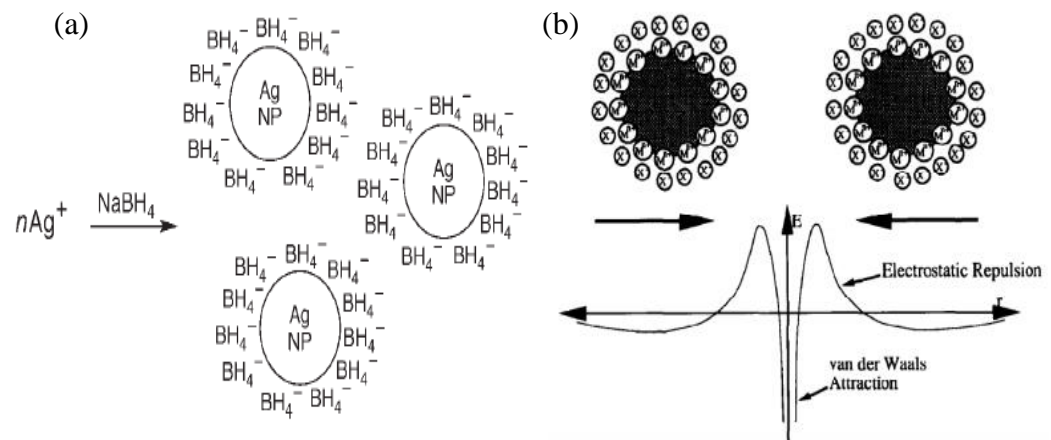
Figure 4.3: Schematic diagram represents (a) absorption of BH_4^- ion layer to the surface of silver nanoparticles (b) electrostatic repulsion (Singh, et al., 2018).

4.1.2   Effect of concentration of capping agent

The concentration of the capping agent or stabilizer, 1-dodecanthiol (DDT) does affects the particle size of synthesized silver nanoparticles. In order to study and investigate the effect of concentration of capping agent on the nanoparticles size, silver nanoparticles were prepared with different concentration of capping agent, while the other parameters such as initial concentration of silver nitrate, concentrating of sodium borohydride and reaction temperature were kept constant at 0.02 M, 0.36 M and 0 ^{o}C respectively.
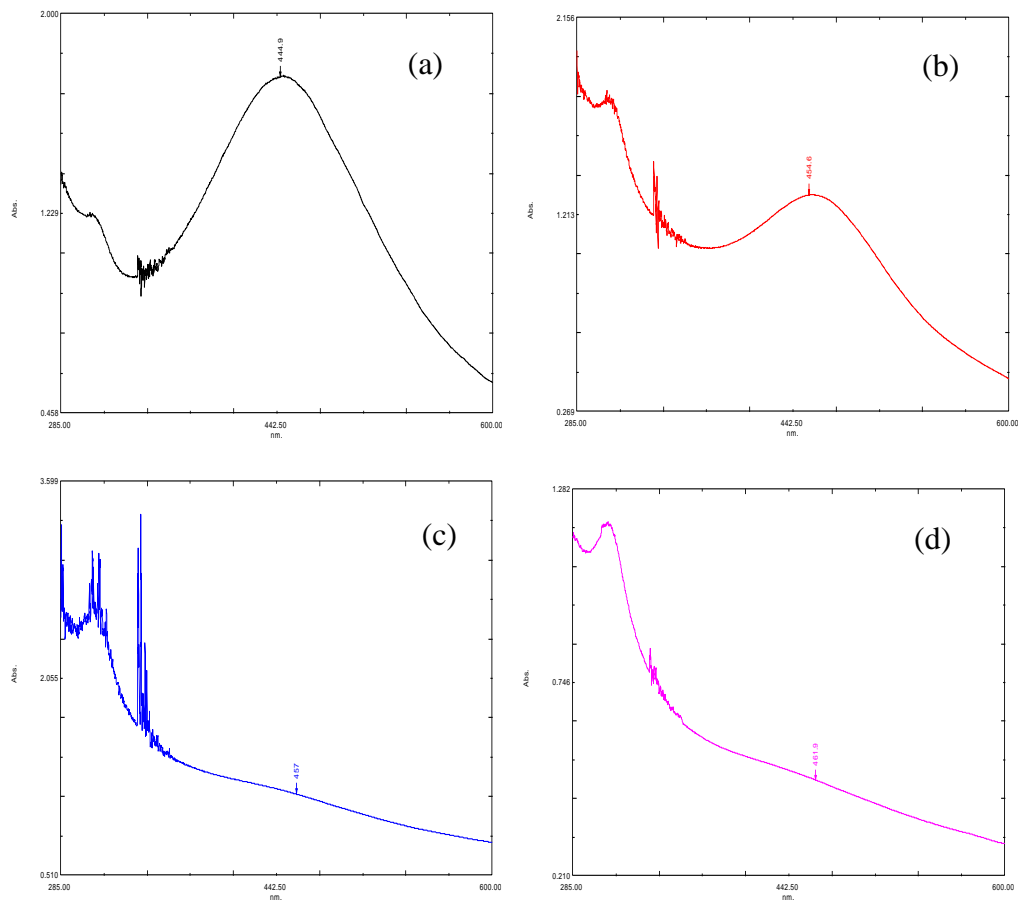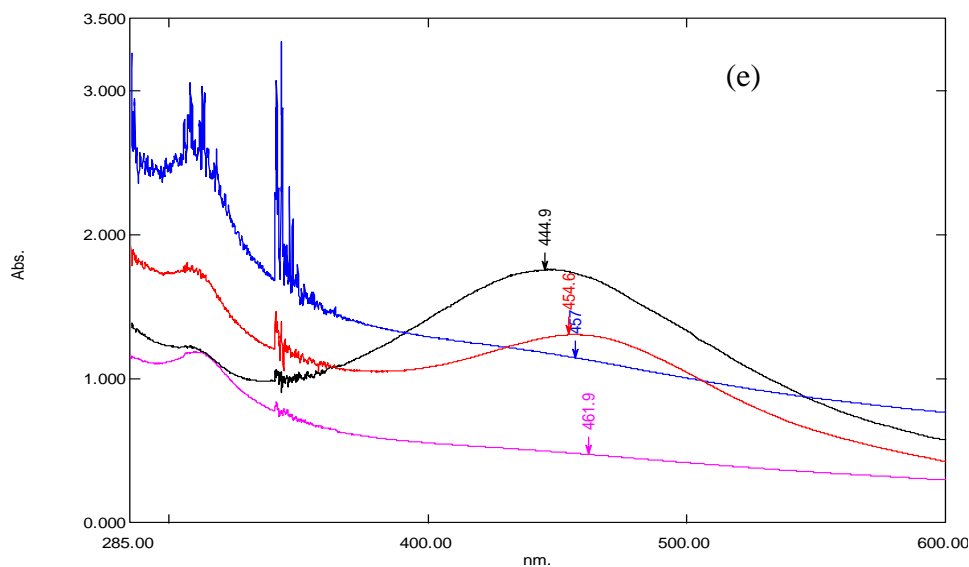
Figure 4.4: UV/Vis spectrum of silver nanoparticles solution which were synthesized with different concentration of capping agent, (a) 0.052 M (b) 0.106 M (c) 0.212 M (d) 0.318 M (e) combination of spectra of (a) to (d).

Table 4.2: Absorbance and wavelength obtained from UV/Vis spectrum of silver nanoparticles solutions corresponding to S value with calculated E_{bg}

S value	Concentration of DDT (M)	Absorbance	Wavelength (nm)	E_{bg} (eV)
0.5	0.052	1.7559	444.90	2.79
1.0	0.106	1.3112	454.60	2.73
2.0	0.212	1.1216	457.00	2.72
3.0	0.318	0.4780	461.50	2.69

Figure 4.4 shows UV/Vis spectra of silver nanoparticles solutions which were synthesized with different concentrations of capping agent, and with the S values of 0.5, 1.0, 2.0 and 3.0. The informations obtained from the UV/Vis specta were summarized in Table 4.2. The band gap energy, E_{bg} of silver nanoparticles were calculated and tabulated in Table 4.2. From the specta obtained, it can be seen that the silver nanoparticles give a plasmon peak at the range of 444-462 nm which falls in the given theoretical range of 415-465 nm. Based on the plasmon peaks obtained, it proved that the silver nanoparticles have been synthesized successfully. For the spectrum of silver nanoparticles which were synthesized with lower concentration of capping agent, S value of 0.5, it can be deduced that the shape of the silver nanoparticles synthesized is spherical since there is only one resonance absorption peak being observed.

From the spectra obtained, it can be found that the measured absorbance of the plasmon peaks showed decrease from 1.7559 to 0.4780 when the concentration of capping agent increases from 0.052 M to 0.318 M. According to Mie scattering theory, the results obtained in the study show that silver nanoparticles with bigger size have been synthesized as indicated by the decrement of measured absorbance. This is because the larger the particle size, less light is scattered by particles and thus less incident light has been absorbed. Hence, smaller value of measured absorbance indicates that the bigger size of silver nanoparticles are produced. Moreover, with the increasing of concentration of stabilizer, the incident light scattered and absorbed by the silver nanoparticles decreases due to interference of

stabilizer. At the same time, the plasmonic effect of the silver nanoparticles will decrease as well. Therefore, it can be observed that the noise peaks between the wavelengths of 285-370 nm which are given by DDT become stronger with increasing absorbance until the absorption plasmon peak of the synthesized silver nanoparticles is diminished. Based on the information obtained from the spectra, the smallest size of silver nanoparticles (20-70 nm) are able to be synthesized with 0.052 M concentration of stabilizer while the largest size of silver nanoparticles (above 800 nm) can be produced with 0.318 M concentration of stabilizer. These result will be further proved and consolidated by the results obtained from SEM analysis.

By using the calculated band gap energy, E_{bg}, it also can be concluded that the excess amount of capping agent will increase the silver nanoparticles in term of size. When the band gap energy decreases, the absorption plasmon peak wavelength increases and this phenomena is known as red shift. Generally, red shift phenomena is always associated with increasing of nanoparticle size. According to summarized results in Table 4.2, the wavelength of the plasmon peak shifted from 444.90 nm to 461.50 nm with the increment of concentration of capping agent, S value from 0.5 to 3.0 while the calculated E_{bg} decreases from 2.79 eV to 2.69 eV. In addition, according to Einstein's photon energy equation which has been shown, the band gap energy has a relationship of indirectly proportional to the wavelength of absorption peak. Samller particle size with larger value of measure absorbance, results in larger value of band gap energy. Even though there is only a slight

decreasing in E_{bg}, but it can still serve as an evident to prove that the smallest size of silver nanoparticles can be produced with the concentration of DDT of 0.052 M (S = 0.5).

Theoretically, the smaller size of metallic nanoparticles should be produced by increasing the concentration of capping agent. This is because more stabilizer molecules which serve as protective group are able to attach to the surface of silver nanoparticles and prevent the aggregation and agglomeration between particles through steric stabilization. Thus, the synthesized silver nanoparticles possess of smaller size and they are well-dispersed. However, after reaching of an optimum concentration, instead of decreasing, the size of nanoparticles will grow to larger scale due to the formation of bigger micelle. When excess amount of capping agent is added, which exceeds the critical micelle concentration (CMC), the micelle with larger size will be formed. The larger micelle will destabilize the silver nanoparticles, aggregation will occur and thus the size of silver nanoparticles will increase. Therefore, it can be concluded that the concentration of capping agent, with the S value of 0.5 (0.052 M) is optimum for producing smaller nano-scale of nanoparticles.
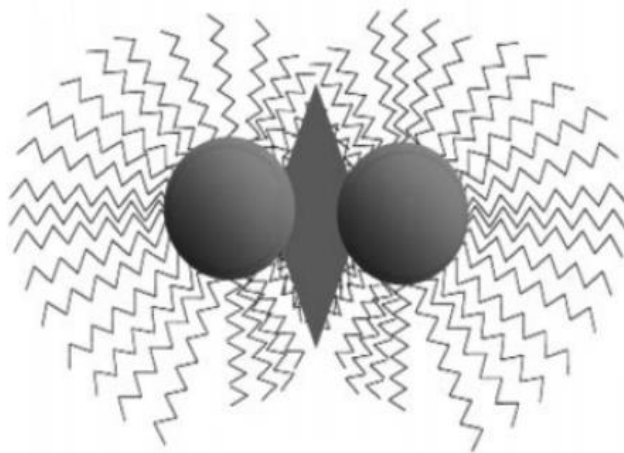
Figure 4.5: Schematic diagram of steric stabilization due to the presence of capping agent (Singh, et al., 2018).

4.2 Scanning Electron Microscopy (SEM)

SEM is an instrument used to study the morphology of the silver nanoparticles synthesized. From the images obtained from SEM, the particle size, shape, distribution, density and surface coverage could be observed, measured and investigated.

4.2.1 Effect of temperature

Particle size of the synthesized silver nanoparticles would be affected by the reaction temperature. In order to investigate the effect of temperature on formation of silver nanoparticles and their particle size, the silver nanoparticles were synthesized at different temperature, at room temperature and in ice bath, while the other parameters such as initial concentration of metal precursor, silver nitrate,

concentration of reducing agent, sodium borohydride and concentration of capping agent, 1-dodecanethiol were kept constant at 0.02 M, 0.36 M and 0.052 M respectively.

(a)　　　　　　　　　　　　　　　　(b)
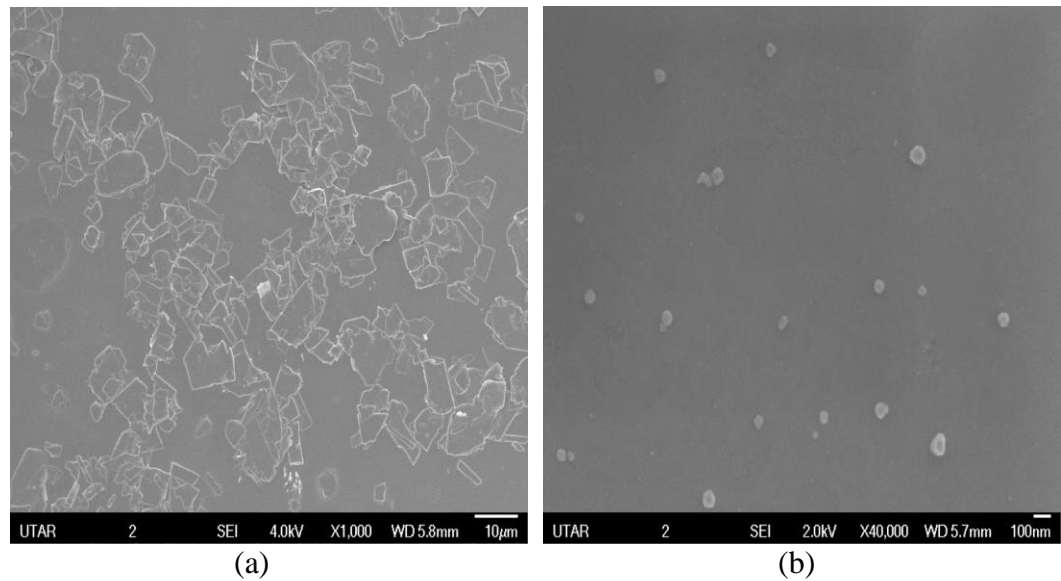
Figure 4.6: SEM images of silver nanoparticles which were synthesized at different temperature (a) room temperature (25 $^{\circ}$C) (b) ice bath (0 $^{\circ}$C).

Figure 4.6 shows the SEM images of silver nanoparticles which were synthesized at two different temperature, namely at room temperature (25 $^{\circ}$C) and in ice bath (0 $^{\circ}$C). Based on the images obtained, the particle size of silver nanoparticles could be measured and determined according to the scale given. The silver nanoparticles with the size of more than 3000 nm were synthesized at room temperature. However, the silver nanoparticles with the size range of 20-70 nm were synthesized in ice bath. It could be seen that there was a great difference in size when the synthesis temperature was different. Meanwhile, the results obtained had proved

that nanoparticles with smaller size could be prepared at lower temperature. On the other hand, it could also be observed that the silver nanoparticles which were synthesized in ice bath possess spherical shape while silver nanoparticles synthesized at room temperature appeared in irregular shape with sharp edge and high crystallinity.

It had been found that the formation of silver nanoparticles occurred in the early synthetic stages, i.e. nucleation and subsequently growth process. Nucleation is the first step in the formation of a thermodynamic new structure or new phase through self-assembly process which grows irreversibly into a nucleus with larger size within the body of a metastable parent phase (Okolieocha, et al., 2015). Nucleation will only take place in a supersaturated solution which is thermodynamically unstable in order to produce small size particles. After forming of the stable nuclei from solution, they grow through adsorption of soluble molecules onto the stable cluster surface is known as molecular addition. Secondary growth occurs when smaller unstable nuclei combine with stable particles, namely aggregation (Pacioni, et al., 2015). Figure 4.7 illustrates La Mer's mechanism for the nucleation and growth process of particles.
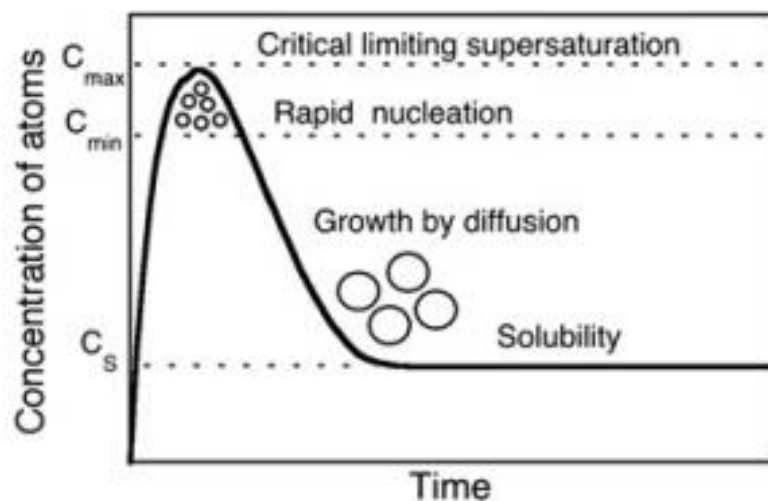
Figure 4.7: Representation for La Mer's mechanism for the nucleation and growth process of particles (Pacioni, et al., 2015).

According to Piñero, et al. (2017), variation of temperature might influence the reaction kinetic, agglomeration and aggregation mechanics, included intra-particle ripening, oriented attachment and overgrowth. When the synthetic reaction is carried out at high temperature, there is an increment in rate of reduction reaction and reduction kinetic. According to classical La Mer's mechanism, the atoms will then aggregate to particles. Meanwhile, nucleation and growth process of silver nanoparticles will be accelerated. The silver nanoparticles will grow and aggregate during secondary growth process. High temperature increases the rate of reduction of silver metal salt and forms silver particles due to high effective collision between the particles. The silver particles can be produced at shorter time at high temperature. However, due to high reduction kinetic, the stabilizer or capping agent is not able to attach to the surface of particles immediately and spontaneously. Without the attachment of the protective group, the nanoparticles will suffer

aggregation and agglomeration and thus, larger size of nanoparticles will be produced. On the other hand, the rate of reduction decreases at low temperature, nucleation and growth of nanoparticles will also slow down. The stabilizer molecules are able to be adsorbed to the surface of nanoparticles and protect them from aggregation and agglomeration. Thus, silver nanoparticles with smaller size are formed.

4.**2.2**   **Effect of concentration of capping agent**
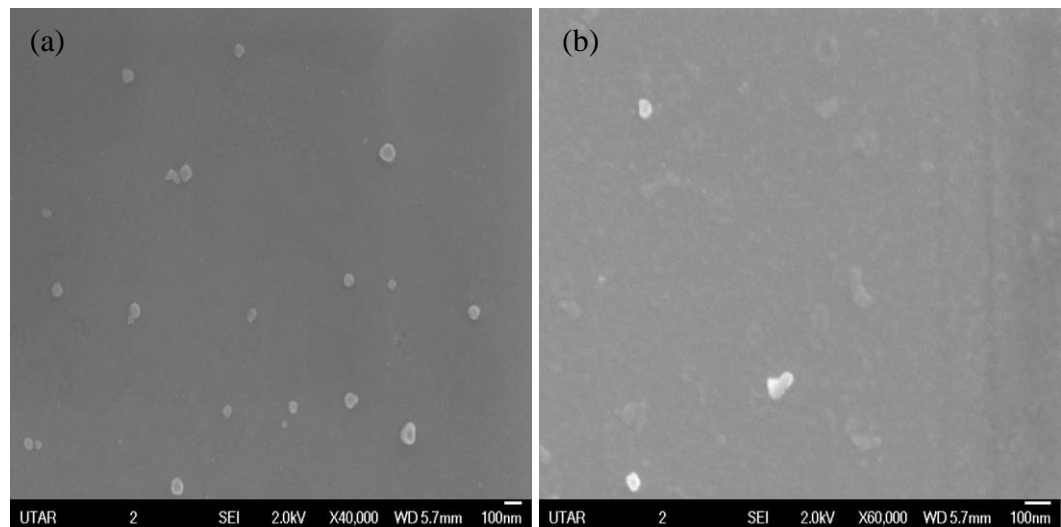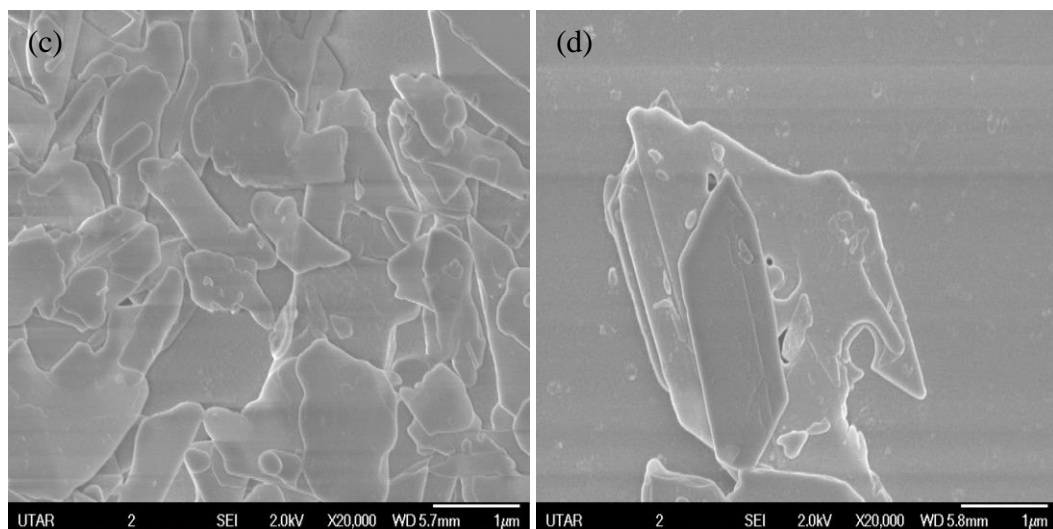
Figure 4.8: SEM images of silver nanoparticles which were synthesized with different concentration of capping agent, with the S value of (a) 0.5 (b) 1.0 (c) 2.0 (d) 3.0.

Table 4.3: The size of synthesized silver nanoparticles corresponding to S value

S value	Concentration of DDT (M)	Particle size (nm)
0.5	0.052	20-70
1.0	0.106	40-100
2.0	0.212	Above 350
3.0	0.318	Above 800

Figure 4.8 shows the SEM images of the silver nanoparticles which were synthesized with different concentration of capping agent and their particles size were measured and tabulated in Table 4.3. The SEM images further confirm and prove the discussion and conclusion made in the UV/Vis spectrophotometry part, an adequate amount of capping agent, DDT (0.052 M) should be added during the synthesis of silver nanoparticles in order to produce the silver nanoparticles of the smallest size, 20-70 nm. With increasing concentration of capping agent from 0.052 M to 0.318 M, the silver nanoparticles grow to larger size. Meanwhile, silver nanoparticles with spherical shape can be synthesized with suitable amount of stabilizer. From the SEM images, it can be seen that silver nanoparticles with smaller size, that is less than 100 nm possess a spherical structure while the silver nanoparticles with larger size, i.e. above 300 nm, possess an irregular structure due to agglomeration and aggregation.

4.3   Atomic Force Microscopy (AFM) and Light Microscopy (LM)

AFM and LM are the instruments used for studying the surface morphology, particle density and surface coverage, of synthesized silver nanoparticles which were coated on the surface of a glass substrate by applying of coupling agent, MPTMS.
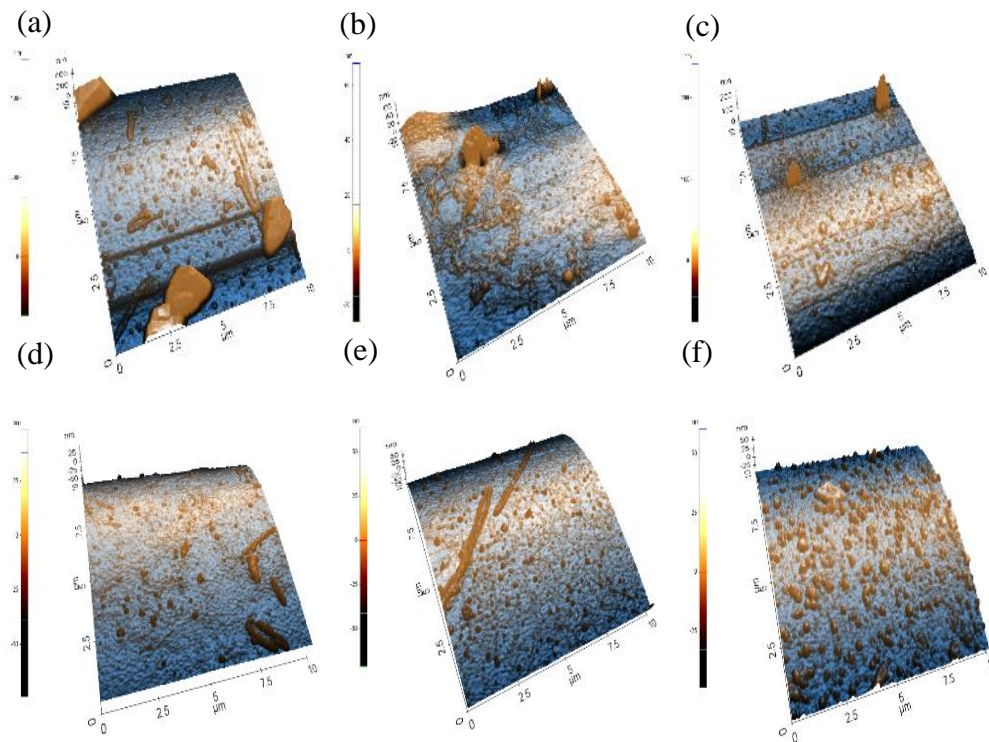
Figure 4.9: AFM images of AgNPs which were synthsized with different S value and coated on surface of substarte with different volume % of coupling agent: (a) S = 0.5, C.A. = 1% (b) S = 0.5, C.A. = 3% (c) S = 0.5, C.A. = 5% (d) S = 3.0, C.A. = 1% (e) S = 3.0, C.A. = 3% (f) S = 3.0, C.A. = 5%.
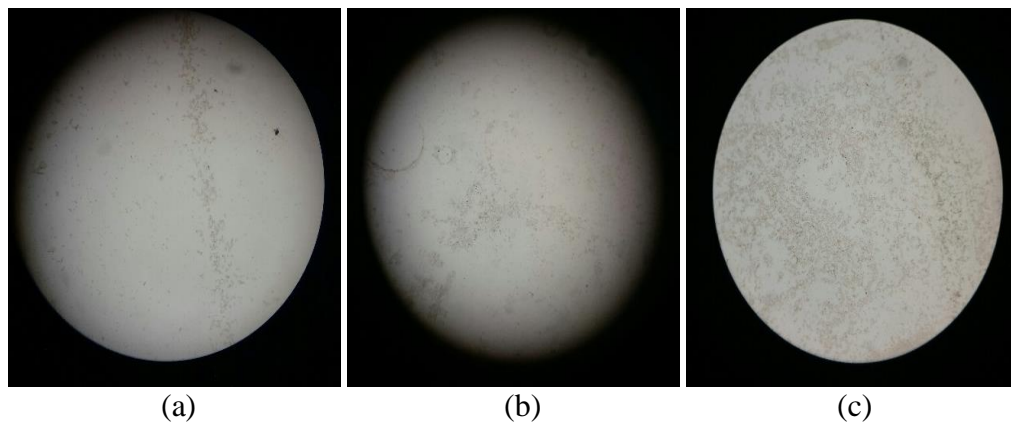
Figure 4.10: LM images of syntehsized silver AgNPs coated on glass substrate by applying different volume % of coupling agent of (a) 1% (b) 3% (c) 5%.

Figure 4.9 and 4.10 show the AFM and LM images of syntehsized AgNPs which were coated on the sruface of a glass substrate by applying the different volume % of coupling agent namely MPTMS. It can be observed that when the volume % of the coupling agent increases, more AgNPs are coated on the substrate and also the distribution of AgNPs on substrate is more even. When more coupling agent was employed, the surface coverage of AgNPs was higher. The silanol group (Si-OCH$_3$) present in the terminal end of MPTMS will reatc with the Si-OH group on the surface of treated glass substrate and a siloxane Si-O-Si bond is formed. This siloxane bond strongly attaches both glass substrate and the coupling agent. On the other terminal of MPTMS molecule, the thiol group (-SH) serves as an incresdible anchor for AgNPs. Therfore, when the concentration of coupling agent increases, more coupling agent will be bonded to the surface of substrate through siloxane, Si-O-Si bonds. Meanwhile, more of the AgNPs can be attached to the surface of glass subtrate through thiol group of MPTMS. The Figure 4.11 shows the overall bonding process of MPTMS which serves as an adhesion promoter to improve the binding of organic materials on inorganic substrate.
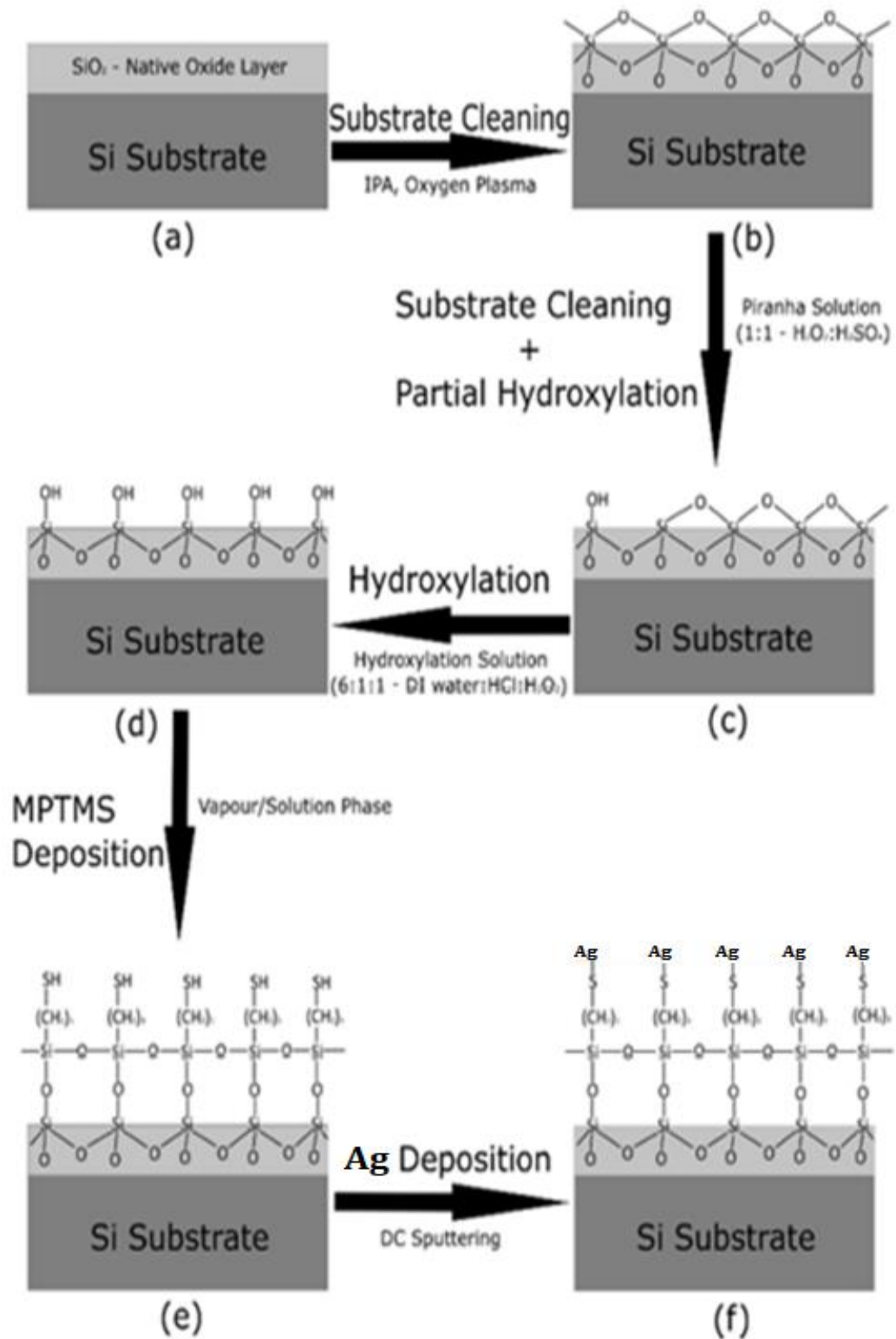
Figure 4.11: Overall coating process of AgNPs on surface of Si substrate by applying of MPTMS as adhesion promoter (Gothe, et al., 2018).

4.4   X-ray Diffraction (XRD)
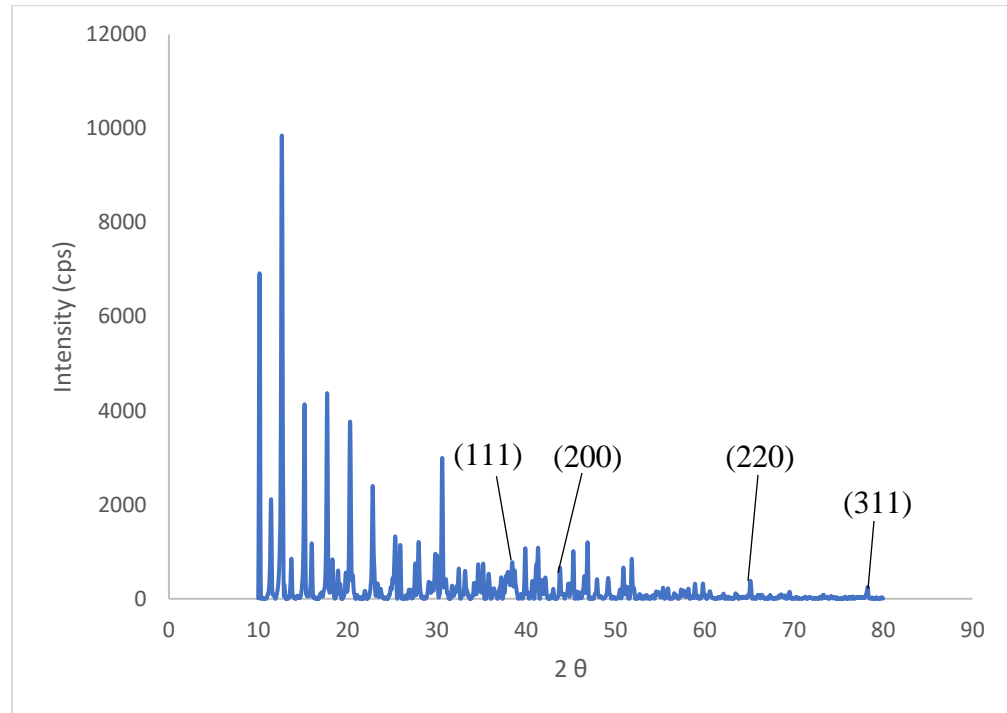
Figure 4.12: XRD pattern of synthesized AgNPs.

Figure 4.12 shows the XRD pattern of AgNPs which were synthesized with R value of 18, S value of 1.0 and at 0 °C. The diffraction peaks at 38.37°, 44.65°, 65.02° and 78.17° were assigned to (111), (200), (220) and (311) respectively. According to Fredrick and Mangaka (2016), the similar results of diffraction peaks of AgNPs at 38.08° (111), 44.18° (200), 64.30° (220) and 77.23° (311) have been reported. All the diffraction peaks showed in the XRD pattern as mentioned are corresponding to face centred cubic (FCC) structure of synthesized silver nanoparticles and also indicates the crystalline nature of AgNPs. However, the lower intensity of the diffraction peaks indicate that the synthesized AgNPs are low in crystallinity. There

is a slight shifting of the 2θ value of the diffraction peaks obtained in this study which could be due to different type of capping agent used.

On the other hand, the data obtained from XRD analysis have been phase analyzed using instrument software to compare with the reference database from International Centre for Diffraction Data (ICDD). Based on the phase analysis report, it proves that the substances that have been synthesized is AgNPs. The phase analysis report is shown in Appendix C. The XRD pattern shows that there are other diffraction peaks present which might be due to the presence of impurities, such as unreacted starting materials and by-products. Meanwhile, the size of synthesized AgNPs can be calculated via Debye-Scherrer equation using the information obtained from XRD pattern as shown in Appendix D. The average size of synthesized AgNPs is found to be 50.66 nm at 38.37°. The calculated size of AgNPs is consistent with the result obtained from SEM, which the AgNPs with sizes range between 40-100 nm were produced.

4.5   Optical property of silver nanoparticles

Figure 4.13: The silver nanoparticles solutions which were synthesized from different concentration of stabilizer, S value of 3.0, 2.0, 0.5, and 1.0 (from left to right).

Figure 4.13, shows that silver nanoparticles solutions with different colours were synthesized with different concentration of stabilizer via the chemical reduction method with the use of a fixed amount of sodium borohydride as reducing agent. Based on the results obtained from UV/Vis spectroscopy and SEM, the silver nanoparticles which were synthesized with concentration of stabilizer, with the S value of 0.5 have the smallest size range of 20-70 nm, followed by S value of 1.0 (40-100 nm), 2.0 (above 350 nm) and subsequently 3.0 (above 800 nm). By comparing with Figure 4.13, the dark brown colour solution indicates the silver nanoparticles with smaller size. With the increasing of particle size, the silver

nanoparticles solutions turn from dark brown to light brown, then to yellow. The optical colour results obtained in the study match the results that are reported by Song, et al. (2008).

The colour of silver nanoparticle solutions varies from each other according to their particles size. This is mainly due to the localized surface plasmon resonance (LSPR) effect of metallic nanoparticles. According to Mavani and Shah (2013), the LSPR of a metallic nanoparticles is highly dependent on their particles size and shape. When the nanoparticles start to aggregate, agglomerate and grow to larger scale, the optical properties of silver nanoparticles will change. When the particle size increases, the LSPR shifts to lower energy. The scattering and absorption peaks of silver nanoparticles shift to longer wavelength. The conduction electrons which are closer to the surface of particles will delocalized and they are shared amongst neighboring particles. Thus, silver nanoparticles with different sizes will have different oscillation resonance. The statements explain the dependency of the colour outlook of synthesized silver nanoparticles by particles size and shape.

4.6   Attenuated Total Reflectance (ATR) and Fourier-Transform Infrared Spectroscopy (FTIR)

FTIR and ATR are the instruments that are used to determine the functional groups in 1-dodecanthiol (DDT), 3-(Trimethoxysilyl)-1-propanethiol (MPTMS) and DDT-functionalized silver nanoparticles. It can be proved the presence of thiol functional groups (-SH) and confirmed that the thiol stabilizer is functionalized the silver nanoparticles through IR spectrum.

Figure 4.14 show the IR spectrum of both DDT and DDT-functionalized AgNPs, while the data extract from IR spectrum of DDT and DDT-functionalized AgNPs are summarized and tabulated in Table 4.4. For IR spectrum of DDT, there are few important peaks occur in spectrum which indicates that the pure DDT were employed in the synthesis of silver nanoparticles. The structural formula of DDT is shown in Figure 4.15. The peaks appear at 2921 and 2852 cm^{-1} correspond to C-H stretch. Besides that, the peaks shown at 1465 cm^{-1} and 1377 cm^{-1} indicate that the methylene group, C-H$_2$ bend and methyl group, C-H$_3$ bend are present in the structure of DDT. Another important peak appears at 721 cm^{-1} arises from C-S bend which indicates that the thiol group is present in the DDT.

(a)

(b)
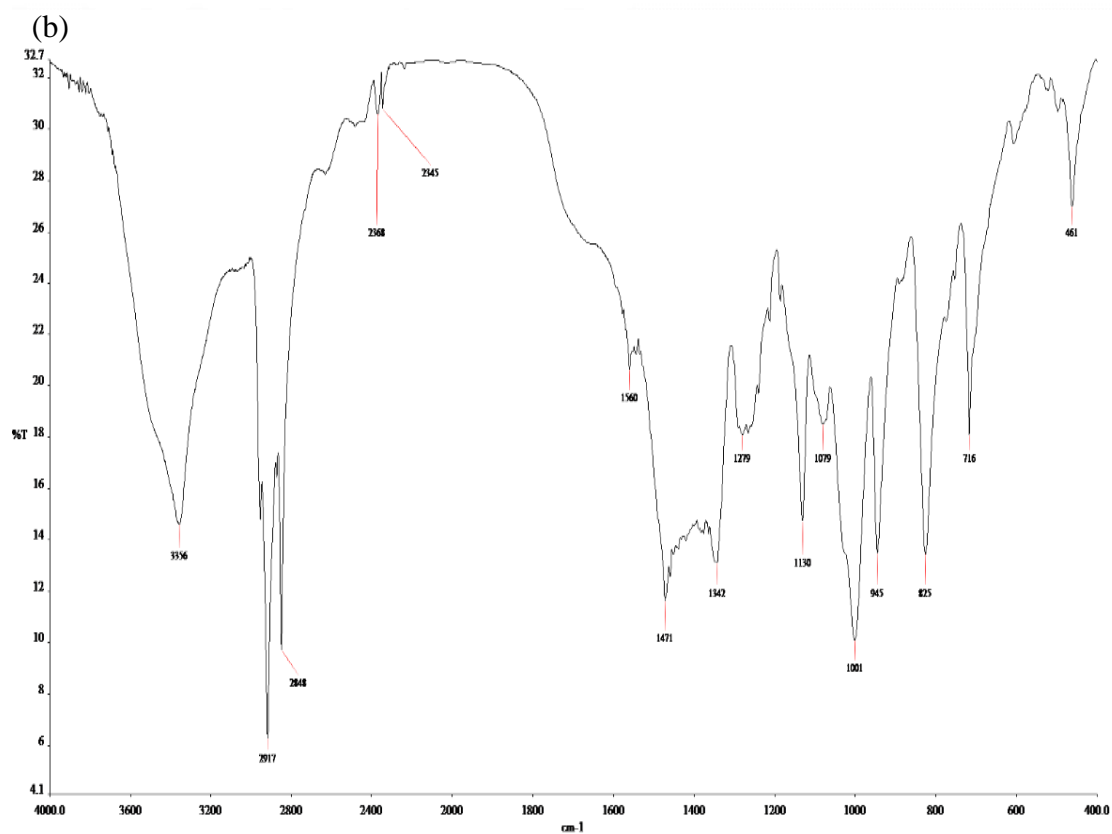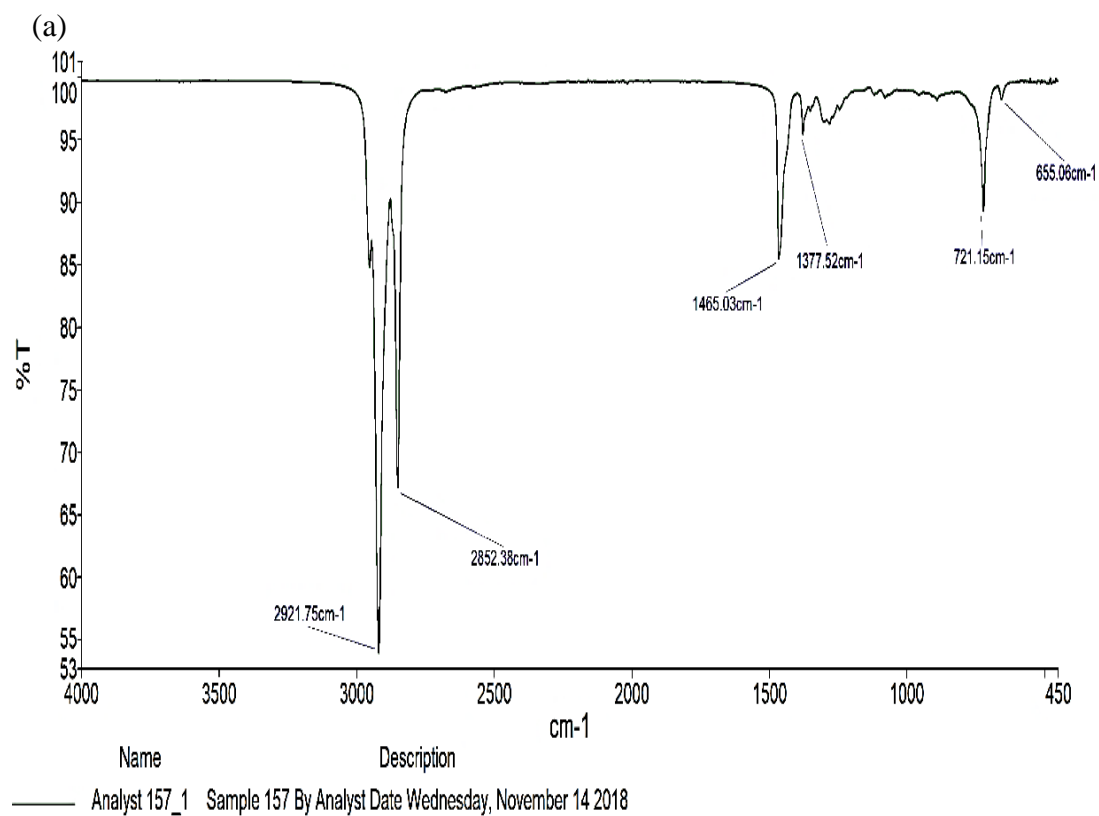
Figure 4.14: IR spectrum of (a) DDT (b) DDT-functionalized AgNPs.

Table 4.4: IR spectrum data of DDT and DDT-functionalized AgNPs

Sample	Wavenumber (cm^{-1})	Type of vibration
	2921, 2852	C-H stretch
	1465	C-H$_2$ bend
DDT	1377	C-H$_3$ bend
	721	C-S bend
	2917, 2848	C-H stretch
	1471	C-H$_2$ bend
DDT-functionalized	1342	C-H$_3$ bend
AgNPs	716	C-S bend
	2368, 2345	S-H stretch
	3356	O-H stretch
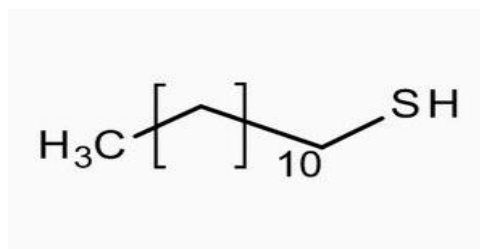
Figure 4.15: Structural formula of DDT.

By comparison, the important peaks showed in the IR spectrum of DDT are also appear in the spectrum of DDT-functionalized AgNPs. The peaks appear at 2917 and 2848 cm^{-1} arise from C-H stretch. Moreover, the present of functional groups of C-H$_2$ bend and C-H$_3$ bend is confirmed by the peaks value at 1471 and 1342 cm^{-1}. Experimental wavenumber obtained for C-S bend, 716 cm^{-1} agrees with the theoretical range. Other than that, there are other significant peaks that occur at 2368 and 2345 cm^{-1} correspond to S-H stretch which have confirm that the DDT serves as a protective group and attaches to the surface of AgNPs to prevent them from aggregation and agglomeration. Some of the peaks showed in AgNP solution incorporated with DDT are shifted which might be due to the twisting, wagging the rocking of the bond chain. However, there is one peak appears at 3356 cm^{-1} which is only present in the IR spectrum of DDT-functionalized AgNPs but absent in IR spectrum of pure DDT. The occurrence of this peak indicates the present of hydroxyl group, O-H stretch in the structure of DDT-functionalized AgNPs which might be due to the presence of moisture in the silver nanoparticles sample.

Figure 4.16 shows the IR spectrum of pure MPTMS while the spectrum data obtained have summarized in Table 4.5. The presence of methyl group, is found in the structure of MPTMS by the peaks shown at 2940.14, 2840.87 cm^{-1}. Moreover, the peaks appear at 1187.14 and 1076.53 cm^{-1} show the C-O stretching vibration of MPTMS. In addition, both peaks occur at 798.97 and 460.90 cm^{-1} correspond to Si-O stretching and Si-O bending respectively. The peaks shown in the IR spectrum

prove that pure MPTMS was employed for the coating of silver nanoparticles on the surface of a glass substrate.
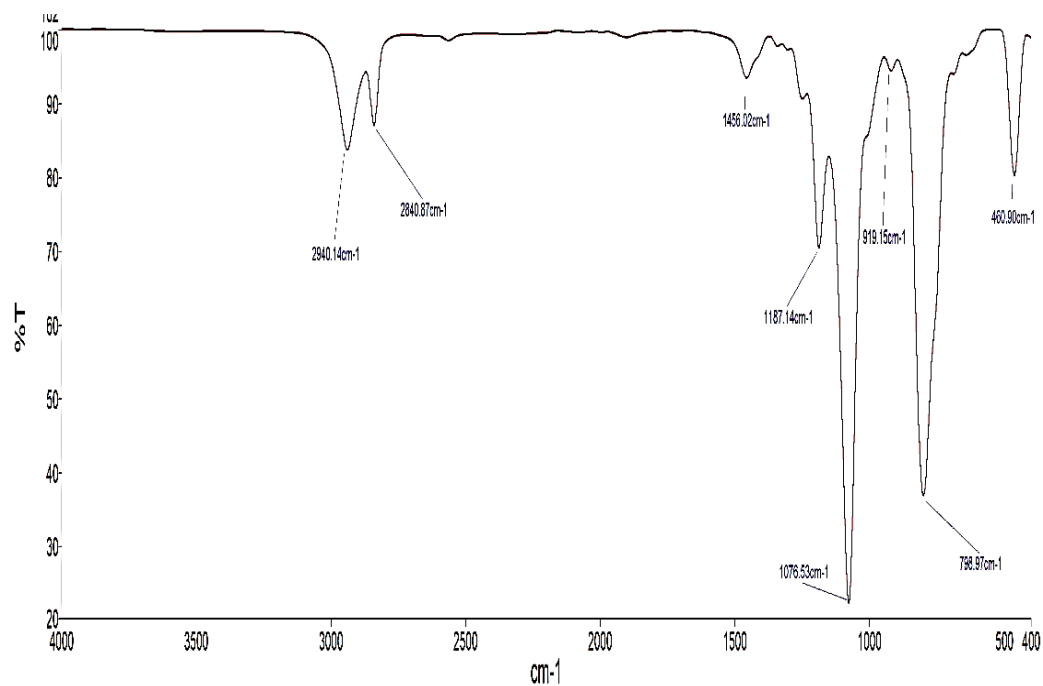
Figure 4.16: The IR spectrum of pure MPTMS.

Table 4.5: IR spectrum data of pure MPTMS

Sample	Wavenumber (cm^{-1})	Type of vibration
	2940.14, 2840.87	C-H stretch
	1456.02	C-H$_2$ bend
MPTMS	1187.14, 1076.53	C-O stretch
	798.97	Si-O stretch
	460.90	Si-O bend

4.7 Percentage yield

The silver nanoparticles were synthesized by means of chemical reduction method, using sodium borohydride as reducing agent with 1-dodecanthiol as capping agent. The percentage yield of synthesized silver nanoparticles is 36.08 %. Meanwhile, the concentration of synthesized silver nanoparticles was determined and calculated, 7.21 x 10^{-3} M. The calculation of percentage yield and concentration of silver are shown in Appendix E. There might some experimental errors that cause in low percentage yield, such as weight loss due to transferring the silver nanoparticles solution from one glassware to another and during washing process with ethanol to remove the impurities from silver nanoparticles.

4.8 Light harvesting efficiency of solar cell

The current, voltage and power of bare solar cell and solar cells coated with AgNPs which were produced using different concentration of capping agent, S value and applying various volume % of coupling agent, were measured and recorded using DC Electronic Load UV Tester. The improvement percentage of the light harvesting efficiecny of solar cells are calculated as shown in appendix F.

Table 4.6: Power output and improvement percentage of solar cells coated with AgNPs solution which was synthesized using different S value of DDT, with 5% of MPTMS

Solar cell	Voltage (V)	Current (A)	Power (W)	Increment (W)	Improvement (%)
Bare	4.496	0.028	0.125	-	-
S = 0.5	4.353	0.057	0.248	0.123	98.40
S = 1.0	4.400	0.056	0.246	0.121	96.80
S = 2.0	4.417	0.059	0.259	0.134	107.2
S = 3.0	4.328	0.057	0.255	0.130	104.0

(a) Power Output of Soalr Cell

(b) Graph of Improvement vs S value
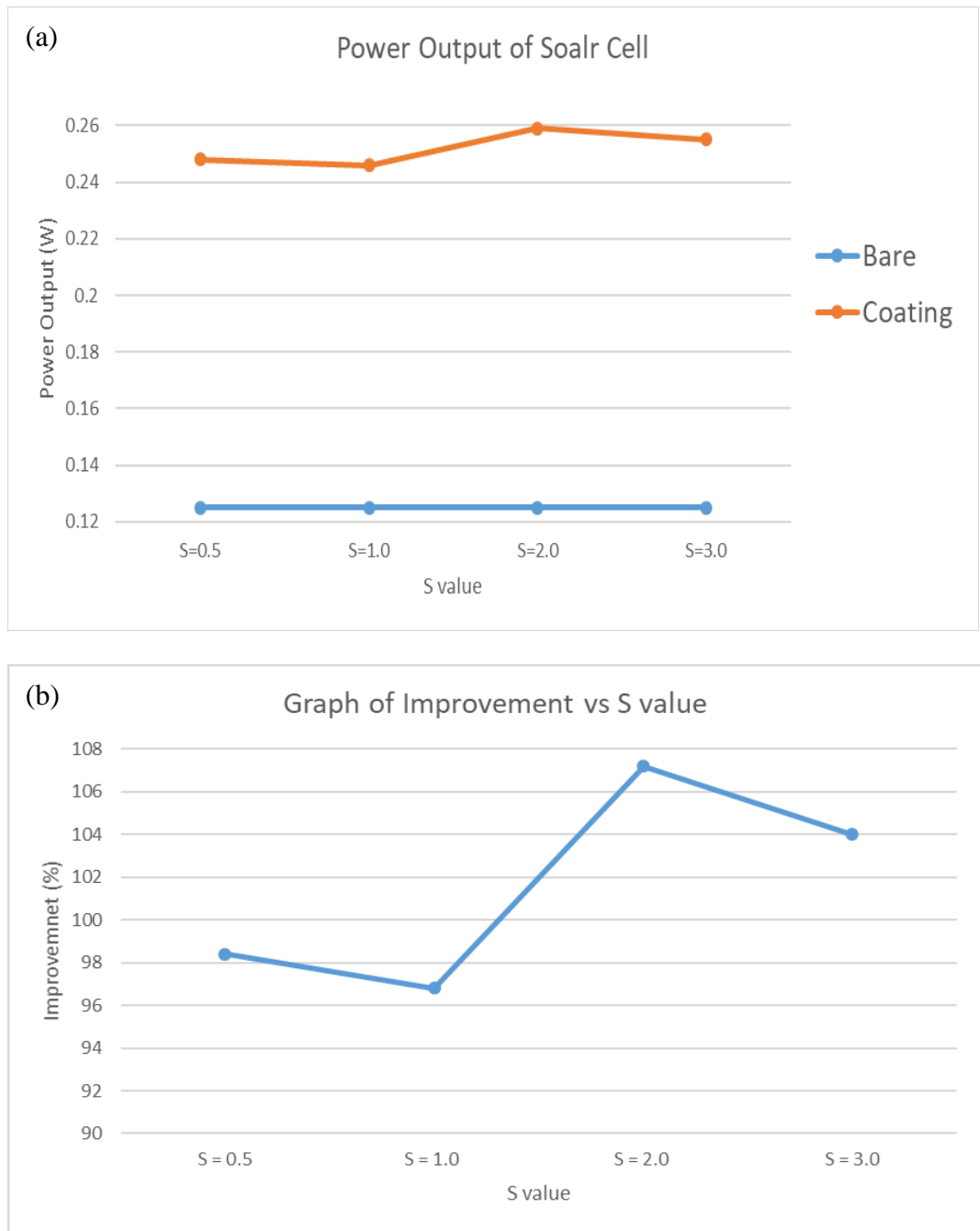
Figure 4.17: Graphs of power output of solar cell and its percentage improvement.

The power output of solar cells coated with AgNPs solution which was synthesized from different concentration of stabilizer, DDT and their power output increment and improvement percentage of light harvesting efficiency are summarized in Table

4.6. Meanwhile, Figure 4.17 shows the plotted graphs of power output of solar cell and its percentage improvement. Based on the data obtained, it can be seen that the solar cell coated with AgNPs solution, which was synthesized with the concentration of DDT, 0.052 M (S value = 2) and the concentration of NaBH$_4$, 0.36 M (R value = 18), at 0 ^{o}C shows the greatest enhancement of 107.2 %, with an improvement of 0.134 W compared to bare solar cell.

Table 4.7: The power output and improvement percentage of solar cells coated with synthesized AgNPs by applying different volume % of coupling agent

Solar cell	Voltage (V)	Current (A)	Power (W)	Increment (W)	Improvement (%)
Bare	4.496	0.028	0.125	-	-
C.A. 1%	3.814	0.057	0.217	0.092	73.60
C.A. 3%	3.811	0.059	0.224	0.099	79.20
C.A. 5%	4.328	0.057	0.255	0.130	104.0
C.A. 7%	4.440	0.059	0.261	0.136	108.8
C.A. 9%	4.129	0.061	0.251	0.126	100.8
C.A. 11%	3.984	0.057	0.227	0.102	81.60
C.A. 13%	4.121	0.055	0.226	0.101	80.80
C.A. 15%	4.110	0.055	0.226	0.101	80.80

(a)

Power Output of Soalr Cell

(b)

Graph of Improvement vs Volume % of Coupling Agent
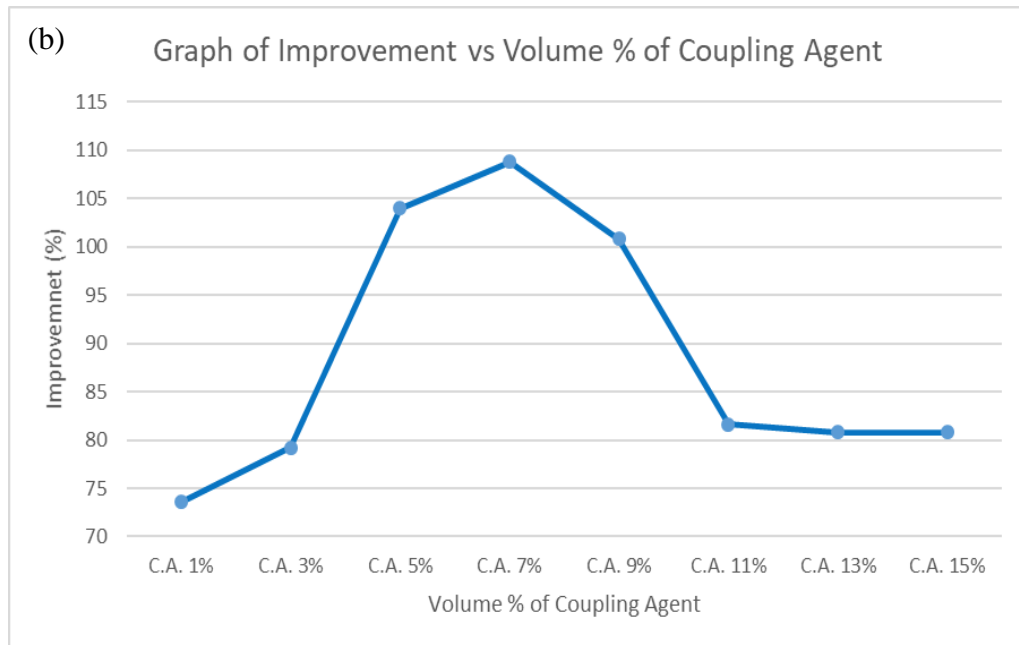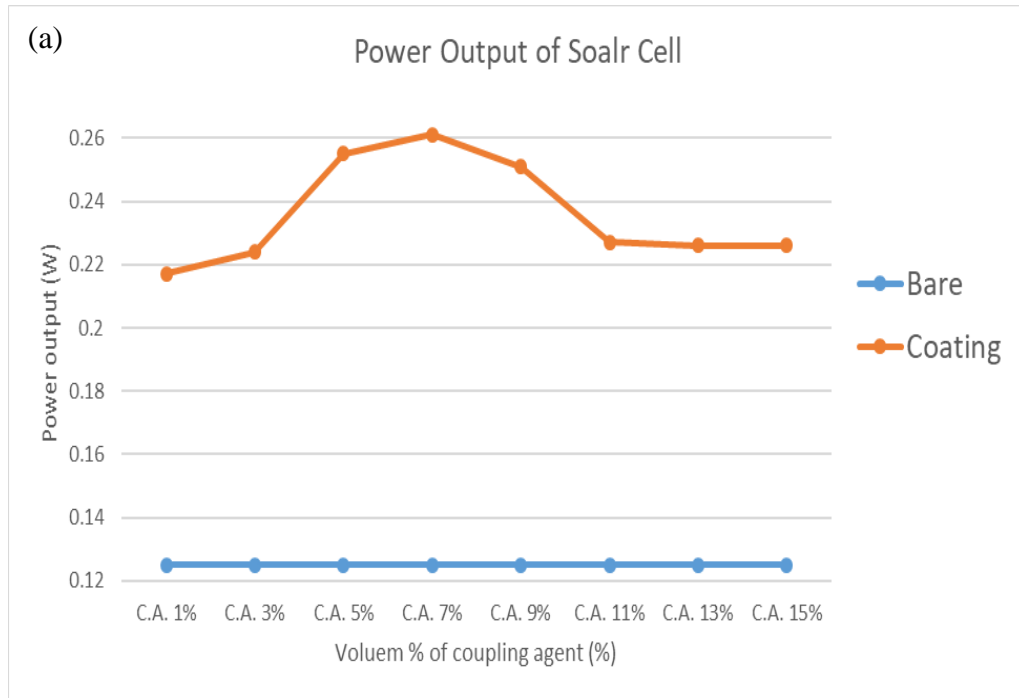
Figure 4.18: Graphs of power output of solar cells and their percentage improvement.

The power output of solar cells coated with AgNPs solution which was synthesized with concentration of DDT, 0.318 M (S value = 3) and concentration of $NaBH_4$, 0.38 M (R value = 18), and by applying different volume % of MPTMS, was measured and recorded. The power output increment and improvement percentage of light trapping efficiency of solar cell are calculated as shown in Appendix F and summarized in Table 4.7.

Figure 4.18 shows the plotted graphs of the power output of solar cell and its percentage improvement. From the data obtained, it can be observed that with the increasing volume % of the coupling agent, the light harvesting efficiency increases as well. This is because the higher the volume % of coupling agent, the higher the surface coverage of AgNPs on solar cell. Hence, more AgNPs can be attached by the coupling agent and form a monolayer on the surface of solar cell. As a result, less reflection of light and more incident light is absorbed by solar cell.

The solar cell prepared as mentioned above but, by applying 7% MPTMS shows the greatest improvement of 108.8 %, with the power output enhancement of 0.136 W compared to the bare solar cell. This might due to a better surface coverage of solar cell deposited with AgNPs at this volume % of coupling agent. The high concentration of MPTMS prevents the shift in plasmon resonance of AgNPs. However, after reaching the optimum volume % of coupling agent (7 %), the enhancement percentage of light trapping efficiency decreases with the increase of volume % coupling agent. This could be due to the formation of bilayer or

multilayer of AgNPs on the surface of solar cell which might have blocked the light from entering into the photoactive layer of the solar cell. Thus, less light was being absorbed. When the volume % of coupling agent reaches 11 % and beyond, the improvement remain at about 81 %.

According to Lee, et al. (2017), depositing a monolayer of AgNPs on the surface of solar cell can significantly improve the light trapping efficiency of solar cell due to LSPR. LSPR only occurs when the incident light frequency matches the conduction electrons oscillation frequency. Hence, the silver nanoparticles integrated on the surface of solar cell will scatter the light into the active layer of solar cell. As a result, more free carriers, holes and free electrons are generated. The results obtained in this study have proved that the coating of AgNPs on the surface of solar cell increases the light harvesting efficiency of solar cell in the range of 70 - 110%. In fact, other than the size of nanoparticle, there are many factors that will also affect the light harvesting efficiency, such as shape, packing, distribution, thickness, space between particles, angle of light etc.

CHAPTER 5

CONCLUSION

5.1   Conclusion

The silver nanoparticles (AgNPs) were successfully synthesized via chemical reduction method using sodium borohydride as reducing agent and 1-dodecanethiol as capping agent. The smaller AgNPs with average size of 20-70 nm could be synthesized with optimum concentration of $NaBH_4$, 0.36 M (R value = 18), concentration of DDT, 0.052 M (S value = 0.5) and at 0 ^oC. There were a few factors that would affect the formation of AgNPs in term of size and shape. By increasing the concentration of $NaBH_4$ from 0.12 M to 0.36 M, the size of AgNPs decreased. However, when the concentration of DDT was increased from 0.052 M to 0.318 M, the nanoparticle size increased. The synthesized AgNPs were characterized using UV/Vis spectroscopy, FTIR, XRD, SEM, AFM and LM. Based on the UV/Vis spectroscopy, the AgNPs give a plasmon absorption peak in the range of 438-462 nm. Based on IR spectroscopy, the peaks that present in the spectrum of pure DDT also present in the spectrum of DDT-functionalized AgNPs. This proved that AgNPs was stabilized by DDT which protects the nanoparticles from agglomeration. In XRD analysis, the diffraction peaks at 38.37^o, 44.65^o, 65.02^o and 78.17^o were assigned to (111), (200), (220) and (311) respectively,

which correspond to the face centred cubic (FCC) structure of synthesized silver nanoparticles. It also indicates the crystalline characteristic of AgNPs.

MPTMS was used as the adhesion promoter to attach the AgNPs on the surface of glass substrate by increasing the binding strength. When the concentration of MPTMS increased, the AgNPs coated on the surface of glass substrate were packed denser and distributed more evenly. Hence, higher surface coverage of AgNPs on the substrate was obtained. The current, voltage and power output of bare solar cell and solar cells coated with AgNPs were measured using DC Electronic Load UV Tester. The improvement percentage of the light harvesting efficiecny of solar cells were investigated and calculated. Based on the power output results obtained, the optimum conditions which gave the greatest enhancement in light harvesting efficiency was to coat the solar cell with AgNPs synthesized with concentration of $NaBH_4$, 0.36 M (R value = 18), concentration of DDT, 0.052 M (S value = 2), by applying 7 % of MPTMS on the solar cell surface. With increasing of volume % of MPTMS from 1-7%, the light harvesting efficiency of solar cell increased. However, the light trapping efficeicny of solar cell decreased with more than 7% of MPTMS. The results obtained have proved that the coating of AgNPs on the surface of solar cell increased the light harvesting efficiency of solar cell in the range of 70 - 110%.

5.2 Future perspective

Different type and concentration of reducing agent and also stabilizer such as dithiolates, phosphine ligands, etc., can be employed in the synthesis of AgNPs through chemical reduction method. In addition, AgNPs can be synthesized at different parameters and conditions, such as various of pH and temperature. Moreover, other type of coupling agents can be also used to act as adhesion promoter during coating of AgNPs on surface of solar cell to prevent the shift in plasmon resonance of metallic nanoparticles.

Incident photon-to-current (IPCE) test can be performed to further confirm the surface plasmon peak of AgNPs by matching it with UV/Vis spectrum of AgNPs. Besides, The enhancement in light harvesting efficiecny is primarily due to AgNPs induced LSPR effect which can be validated using steady state photoluminescene (PL). Other factors that may affect the light harvesting efficiency of solar cell, are shape, packing, distribution, thickness, space between particles, angle of incident light etc., which can be studied and investugated in future.

REFERENCES

Acharya, R., 2017. Interaction of waves with medium. Satellite Signal Propagation, *Impairments and Mitigation*, pp. 57–86.

Ajitha, B., Reddy, A. K., Reddy, P. S., Hwan, J. J. and Chi, W. A., 2016. Role of capping agents in controlling silver nanoparticles size, antibacterial activity and potential application as optical hydrogen peroxide sensor. *RSC Advances*, 6(42), pp. 36171–36179.

Alaqad, K., and Saleh, T. A., 2016. Gold and Silver Nanoparticles: Synthesis Methods, Characterization Routes and Applications towards Drugs. *Journal of Environmental & Analytical Toxicology*, 6(4).

Alqadi, M. K., Abo Noqtah, O. A., Alzoubi, F. Y., Alzouby, J., and Aljarrah, K., 2014. pH effect on the aggregation of silver nanoparticles synthesized by chemical reduction. *Materials Science-Poland*, 32(1), pp. 107–111.

Anigol1, L. B., Charantimath, J. C. and Gurubasavaraj, P. M., 2017. Effect of Concentration and pH on the Size of Silver Nanoparticles Synthesized by Green Chemistry. *Organic and Medicinal Chemistry International Journal*, 3(5), pp. 1-5.

Barman, B., Dhasmana, H., Verma, A., Kumar, A., Singh, D., and Jain, V., 2018. Fabrication of silver nanoparticles on glass substrate using low-temperature rapid thermal annealing. *Energy & Environment*, 29(3), pp. 358–371.

Biolin Scientific, n.d.. Dip Coating. [online] Available at: https://www.biolinscientific.com/measurements/dip-coating [Accessed 18 March 2019]

Cheah, L. K., 2015. Biosynthesis of nanoparticles and silver nanoparticles. *Bioresources and Bioprocessing*, 2(47), pp. 1-16.

Dada, A. O., Adekola, F. A., Adeyemi, O. S., Bello, O. M., Oluwaseun, A. C. Awakan, O. J. and Grace F. A., 2018. Exploring the Effect of Operational Factors and Characterization Imperative to the Synthesis of Silver Nanoparticles. 9, pp. 165-184.

Dai, H., Li, M., Li, Y., Yu, H., Bai, F., & Ren, X., 2012. Effective light trapping enhancement by plasmonic Ag nanoparticles on silicon pyramid surface. *Optics Express*, 20(4), pp. 502-509.

Elnoby, R. M., Mourad, M. H., Elnaby, S. L. H., and Abou Kana, M. T. H., 2018. Monocrystalline solar cells performance coated by silver nanoparticles: Effect of

NPs sizes from point of view Mie theory. *Optics & Laser Technology*, 10(1), pp. 208–215.

Farrell, Z., Shelton, C., Dunn, C., and Green, D., 2013. Straightforward, One-Step Synthesis of Alkanethiol-capped Silver Nanoparticles from an Aggregative Model of Growth. Langmuir, 29(30), pp. 9291–9300.

Fayaz, M., Balaji, K., Girilal, M., Yadav, R., and Kalaichelvan, P. T., 2010. Biogenic synthesis of silver nanoparticles and their synergistic effect with antibiotics: a study against gram-positive and gram-negative bacteria. *Nanomedicine: Nanotechnology, Biology, and Medicine*, 6(1), pp. 103-109.

Fredrick, O. O., and Mangaka, C. M., 2017. Electrochemical and optical band gaps of bimetallic silver-platinum varying metal ratios nanoparticles. African *Journal of Pure and Applied Chemistry*, 11(1), pp. 1–8.

Gelest.com., 2018. [online] Available at: https://www.gelest.com/wp-content/uploads/Goods-PDF-brochures-couplingagents.pdf [Accessed 18 March 2019].

Gharibshahi, L., Saion, E., Gharibshahi, E., Shaari, A., and Matori, K., 2017. Structural and Optical Properties of Ag Nanoparticles Synthesized by Thermal Treatment Method. *Materials*, 10(4), 402.

Gothe, P. K., Gaur, D., & Achanta, V. G., 2018. MPTMS self-assembled monolayer deposition for ultra-thin gold films for plasmonics. Journal of Physics Communications, 2(3), 035005.

Grzelczak, M., Vermant, J., Furst, E. M., and Liz-Marzán, L. M., 2010. Directed Self-Assembly of Nanoparticles. *ACS Nano*, 4(7), 3591–3605.

Gulati1, S., Sachdeva1, M. and Bhasin, K. K., 2018. Capping agents in nanoparticle synthesis: Surfactant and solvent system. *2nd International Conference on Condensed Matter and Applied Physics*, pp. 030214-1 - 4.

Güzel, R., and Erdal, G., 2018. Synthesis of Silver Nanoparticles. Silver Nanoparticles - Fabrication, Characterization and Applications.

Harish, K. K, Nagasamy, V., Himangshu, B. and Anuttam, K., 2018. Metallic Nanoparticle: A Review. *Biomedical Journal of Scientific & Technical Research, BJSTR*, 4(2), pp. 4.

Hutter, E., and Fendler, J. H., 2004. Exploitation of Localized Surface Plasmon Resonance. *Advanced Materials*, 16(19), pp. 1685–1706.

Iravani, S., Korbekandi, H., Mirmohammadi, S.V. and Zolfaghari, B., 2014. Synthesis of silver nanoparticles: chemical, physical and biological methods. *Research in Pharmaceutical Sciences*, 9(6), pp. 385–406.

Jeng, M., Chen, Z., Xiao, Y., Chang, L., Ao, J., Sun, Y., Popko, E., Jacak, W. and Chow, L., 2015. Improving Efficiency of Multicrystalline Silicon and CIGS Solar Cells by Incorporating Metal Nanoparticles. *Materials*, 8(10), pp. 6761-6771.

Jiang, X. C., Chen, W. M., Chen, C. Y., Xiong, S. X., and Yu, A. B., 2010. Role of Temperature in the Growth of Silver Nanoparticles Through a Synergetic Reduction Approach. *Nanoscale Research Letters*, 6(32), pp. 1-9.

Johans, C., 2002. Electrosynthesis of polyphenylpyrrole coated silver particles at liquid–liquid interface. *Electrochemistry Communications*, 4(3), pp. 227–230.

Jung, J. H., Cheol Oh, H., Soo Noh, H., Ji, J. H., and Soo Kim, S., 2006. Metal nanoparticle generation using a small ceramic heater with a local heating area. *Journal of Aerosol Science*, 37(12), pp. 1662–1670.

Jung, J., Ha, K., Cho, J., Ahn, S., Park, H., Hussain, S. Q. and Yi, J., 2013. Enhancing Light Trapping Properties of Thin Film Solar Cells by Plasmonic Effect of Silver Nanoparticles. *Journal of Nanoscience and Nanotechnology*, 13(12), pp. 7860–7864.

Kagithoju, S., Godishala, V., and Nanna, R. S., 2014. Eco-friendly and green synthesis of silver nanoparticles using leaf extract of Strychnos potatorum Linn.F. and their bactericidal activities. 3 Biotech, 5(5), 709–714.

Kajbafvala, A., Bahmanpour, H., Maneshian, M. H., and Li, M., 2013. Self-Assembly Techniques for Nanofabrication. *Journal of Nanomaterials*, pp. 1–3

Khan, I and Saeed, K., 2017. Nanoparticles: Properties, applications and toxicities. *Arabian Journal of Chemistry*.

Krayden, 2009. Silane Coupling Agent. [e-article] Available at: https://krayden.com/pdf/xia_silane_chemistry.pdf [Accessed 18 March 2019]

Lee, C., Goh, W., Chee, S. and Yik, L., 2017. Augmentation of power conversion efficiency of amorphous silicon solar cell employing poly(methyl methacrylate-co-acrylic acid nanospheres encapsulated with gold nanoparticles. *Journal of Materials Science*, 53(7), pp. 5183-5193.

Leonics, 2017. Basic of Solar Cell, Solar Photovoltaic Modules. [online] Available at: http://www.leonics.com/support/article2_13j/articles2_13j_en.php [Accessed 17 March 2019]

Ma, H., Yin, B., Wang, S., Jiao, Y., Pan, W., Huang, S. and Meng, F., 2004. Synthesis of Silver and Gold Nanoparticles by a Novel Electrochemical Method. *ChemPhysChem*, 5(1), 68–75.

Mavani, K. and Shah, M., 2013. Synthesis of Silver Nanoparticles by using Sodium Borohydride as a Reducing Agent. *International Journal of Engineering Research & Technology, IJERT*, 2(3).

Mirela, D., n.d.. Metallic Nanoparticles. [online] Available at: http://sabotin.ung.si/~sstanic/teaching/Seminar/2009/20091214_Dragomir_MetN P.pdf [Accessed 8 March 2019]

Mizuno, H., Sai, H., Matsubara, K., and Kondo, M., 2012. Light Trapping by Ag Nanoparticles Chemically Assembled inside Thin-Film Hydrogenated Microcrystalline Si Solar Cells. *Japanese Journal of Applied Physics*, 51, pp. 042302.

Natsukil, J., Natsuki1, T. and Hashimoto, Y., 2015. A Review of Silver Nanoparticles: Synthesis Methods, Properties and Applications. *International Journal of Materials Science and Applications*, 4(5), pp. 325-332.

Nersisyan, H. H., Lee, J. H., Son, J. H., Won, C. W., Maeng, D. Y., 2003. A new and effective chemical reduction method for preparation of nanosized silver powder and colloid dispersion. *Materials Research Bulletin*, 3(8), pp. 949–956.

Okolieocha, C., Raps, D., Subramaniam, K., and Altstädt, V., 2015. Microcellular to nanocellular polymer foams: Progress (2004–2015) and future directions – A review. *European Polymer Journal*, 73, pp. 500–519.

Pacioni, N. L., Borsarelli, C. D., Rey, V., and Veglia, A. V, 2015. Synthetic Routes for the Preparation of Silver Nanoparticles. *Engineering Materials*, pp. 13–46.

Parveen, F., Sannakki, B., Mandke, M. and Pathan, H. (2016). Copper nanoparticles: Synthesis methods and its light harvesting performance. *Solar Energy Materials and Solar Cells*, 144, pp. 371-382.

Petryayeva, E., and Krull, U. J., 2011. Localized surface plasmon resonance: Nanostructures, bioassays and biosensing — A review. *Analytica Chimica Acta*, 706(1), pp. 8–24.

Phan, C. M. and Hoang, M. N., 2017. Role of Capping Agent in Wet Synthesis of Nanoparticles. *The Journal of Physical Chemistry A*, 121(17), pp. 3213-3219.

Pilipavicius, J., Chodosovskaja, A., Beganskiene, A., and Kareiva, A., 2015. Silver nanoprisms self-assembly on differently functionalized silica surface. *IOP Conference Series: Materials Science and Engineering*, 77, 012006.

Pyatenko, A., Shimokawa, K., Yamaguchi, M., Nishimura, O. and Suzuki, M., 2004. Synthesis of silver nanoparticles by laser ablation in pure water. *Applied Physics A*, 79(20), pp. 803-806.

Piñero, S., Camero, S., and Blanco, S., 2017. Silver nanoparticles: Influence of the temperature synthesis on the particles' morphology. *Journal of Physics: Conference Series*, 786, 012020.

RGS, 2015. What are Solar Cells? [online] Available at: https://rgsenergy.com/how-solar-panels-work/what-are-solar-cells/ [Accessed 17 March 2019]

Saghaei, J., Fallahzadeh, A. and Saghaei, T., 2016. Vapor treatment as a new method for photocurrent enhancement of UV photodetectors based on ZnO nanorods. *Sensors and Actuators A: Physical*. 24(7), pp. 150–155.

Saladin, K. S., Miller, S. E., n.d.. Light Microscopy. [online] *Biology Reference*. Available at: < http://www.biologyreference.com/La-Ma/Light-Microscopy.html> [Accessed 30 Oct. 2018]

Saleh, T. A., and Gupta, V. K., 2013. Covalent and Non-Covalent Functionalization of Carbon Nanotubes. *Advanced Carbon Materials and Technology*, pp. 317–330.

Samsudina, M. S. N., Rahman, M. M. and Wahid, M. A., 2016. Power Generation Sources in Malaysia: Status and Prospects for Sustainable Development. *Journal of Advanced Review on Scientific Research*, 25(1), pp. 11-28.

Siegel, J., Kvítek, O., Ulbrich, P., Kolská, Z., Slepička, P., and Švorčík, V., 2012. Progressive approach for metal nanoparticle synthesis. Materials Letters, 8(9), pp. 47–50.

Singh, M., Goyal, M., and Devlal, K., 2018. Size and shape effects on the band gap of semiconductor compound nanomaterials. *Journal of Taibah University for Science*, 12(4), 470–475.

SolarGreen, 2019. What is a Solar Cell? [online] Available at: https://www.solargreen.net.au/what-is-a-solar-cell-.html [Accessed 17 March 2019]

SolarServer, 2017. Photovoltaics: Solar Electricity and Solar Cell in Theory and Practice. [online] Available at: http://www.solarserver.com/knowledge/basic-knowledge/photovotaics.thml [Accessed 17 March 2019].

Solomon, S. D., Bahadory, M., Jeyarajasingam, A. V. and Rutkowsky, S. A., 2007. Synthesis and Study of Silver Nanoparticles. *Journal of Chemical Education*, 84(2), pp.322-325.

Song, K. C., Lee, S. M., Park, T. S. and Lee, B. S., 2008. Preparation of colloidal silver nanoparticles by chemical reduction method. *Korean J. Chem. Eng.*, 26(1), pp. 153-155.

Sreeram, K. J., Nidhin, M., and Nair, B. U., 2008. Microwave assisted template synthesis of silver nanoparticles. *Bulletin of Materials Science*, 31(7), pp. 937–942.

Sterman, S. and Marsden, J., 1966. SILANE COUPLING AGENTS. *Industrial & Engineering Chemistry*, 58(3), pp.33-37.

Suresh, A. K., Pelletier, D. A., Wang, W., Moon, J. W., Gu, B., Mortensen, N. P. and Doktycz, M. J., 2010. Silver Nanocrystallites: Biofabrication using Shewanella oneidensis, and an Evaluation of Their Comparative Toxicity on Gram-negative and Gram-positive Bacteria. *Environmental Science & Technology*, 44(13), pp. 5210–5215.

Swami, A., Selvakannan, P.R., Pasricha, R. and Sastry, M., 2004. One-Step Synthesis of Ordered Two-Dimensional Assemblies of Silver Nanoparticles by the

Spontaneous Reduction of Silver Ions by Pentadecylphenol Langmuir Monolayers. *J. Phys. Chem. B*, 108(50), pp. 19269-19275.

The Star, 2015. How electricity is generated in Malaysia. [e-article] Available at: https://www.thestar.com.my/metro/focus/2015/04/22/how-electricity-is-generated-in-malaysia/ [Accessed 18 March 2019]

Tien, D. C., Tseng, K. H., Liao, C. Y., Huang, J. C., and Tsung, T. T., 2008. Discovery of ionic silver in silver nanoparticle suspension fabricated by arc discharge method. *Journal of Alloys and Compounds*, 463(1-2), pp. 408–411.

Tippayawat, P., Phromviyo, N., Boueroy, P., and Chompoosor, A., 2016. Green synthesis of silver nanoparticles in aloe vera plant extract prepared by a hydrothermal method and their synergistic antibacterial activity. *PeerJ*, 4, pp. 2589.

Troupis, A., Hiskia, A., and Papaconstantinou, E., 2002. Synthesis of Metal Nanoparticles by Using Polyoxometalates as Photocatalysts and Stabilizers. *Angewandte Chemie International Edition*, 41(11), pp. 1911.

Tsuji, T., Kakita, T., and Tsuji, M., 2003. Preparation of nano-size particles of silver with femtosecond laser ablation in water. *Applied Surface Science*, 206(1-4), pp. 314–320.

Zaman, M., Ahmad, E., Qadeer, A., Rabbani, G., Khan, Rizwan H., 2014. Nanoparticles in relation to peptide and protein aggregation. *International journal of nanomedicine*, 9(1), pp. 899-912.

Zhang, W., Qiao, X., and Chen, J., 2007. Synthesis of nanosilver colloidal particles in water/oil microemulsion. *Colloids and Surfaces A: Physicochemical and Engineering Aspects*, 299(1-3), pp. 22–28.

Zhang, X. F., Liu, Z. G., Shen, W., and Gurunathan, S., 2016. Silver Nanoparticles: Synthesis, Characterization, Properties, Applications, and Therapeutic Approaches. *International Journal of Molecular Sciences*, 17(9), pp. 1534.

Zi, W., Ren, X., Xiao, F., Wang, H., Gao, F., and Liu, S., 2016. Ag nanoparticle enhanced light trapping in hydrogenated amorphous silicon germanium solar cells on flexible stainless steel substrate. *Solar Energy Materials and Solar Cells*, 144, pp. 63–67.

Appendix A

Calculation for band gap energy, E_{bg} of synthesized silver nanoparticles.

$$E_{bg} = \frac{hc}{\lambda}$$

Where, h is the Planck's constant (6.63×10^{-34} m^2 kg s^{-1}), c is the speed of light (3.00×10^8 ms^{-1}) and λ is the absorption wavelength in UV region.

When R = 12, λ = 440.60 nm,

$$E_{bg} = \frac{\left(6.63 \times 10^{-34} m^2 kgs^{-1}\right) \text{ x } (3.00 \times 10^8 \, ms^{-1})}{451.80 \text{ x } 10^{-9} \, m} = (4.402 \text{ x } 10^{-19}) \text{ x } (6.242 \times 10^{18} \text{ eV})$$

$$= 2.75 \text{ eV}$$

When R = 15, λ = 436.30 nm,

$$E_{bg} = \frac{\left(6.63 \times 10^{-34} m^2 kgs^{-1}\right) \text{ x } (3.00 \times 10^8 \, ms^{-1})}{442.50 \text{ x } 10^{-9} \, m} = (4.495 \text{ x } 10^{-19}) \text{ x } (6.242 \times 10^{18} \text{ eV})$$

$$= 2.81 \text{ eV}$$

When R = 18, λ = 457.80 nm,

$$E_{bg} = \frac{\left(6.63 \times 10^{-34} m^2 kgs^{-1}\right) \text{ x } (3.00 \times 10^8 \, ms^{-1})}{438.30 \text{ x } 10^{-9} \, m} = (4.538 \text{ x } 10^{-19}) \text{ x } (6.242 \times 10^{18} \text{ eV})$$

$$= 2.83 \text{ eV}$$

When S = 0.5, λ = 444.90 nm,

$$E_{bg} = \frac{(6.63 \times 10^{-34} m^2 kgs^{-1}) \text{ x } (3.00 \times 10^8 \ ms^{-1})}{444.90 \text{ x } 10^{-9} \ m} = (4.471 \text{ x } 10^{-19}) \text{ x } (6.242 \times 10^{18} \text{ eV})$$

$$= 2.79 \text{ eV}$$

When S = 1.0, λ = 454.60 nm,

$$E_{bg} = \frac{(6.63 \times 10^{-34} m^2 kgs^{-1}) \text{ x } (3.00 \times 10^8 \ ms^{-1})}{454.60 \text{ x } 10^{-9} \ m} = (4.375 \text{ x } 10^{-19}) \text{ x } (6.242 \times 10^{18} \text{ eV})$$

$$= 2.73 \text{ eV}$$

When S = 2.0, λ = 457.00 nm,

$$E_{bg} = \frac{(6.63 \times 10^{-34} m^2 kgs^{-1}) \text{ x } (3.00 \times 10^8 \ ms^{-1})}{457.00 \text{ x } 10^{-9} \ m} = (4.352 \text{ x } 10^{-19}) \text{ x } (6.242 \times 10^{18} \text{ eV})$$

$$= 2.72 \text{ eV}$$

When S = 3.0, λ = 461.50 nm,

$$E_{bg} = \frac{(6.63 \times 10^{-34} m^2 kgs^{-1}) \text{ x } (3.00 \times 10^8 \ ms^{-1})}{461.50 \text{ x } 10^{-9} \ m} = (4.310 \text{ x } 10^{-19}) \text{ x } (6.242 \times 10^{18} \text{ eV})$$

$$= 2.69 \text{ eV}$$

Appendix B

```
          ***  Basic Data Process  ***

Group     : Standard
Data      : TBY_Set_3

# Strongest 3 peaks
  no. peak   2Theta      d        I/I1   FWHM     Intensity  Integrated Int
      no.    (deg)      (A)              (deg)    (Counts)   (Counts)
   1   3    12.6476    6.99337    100   0.18730   9851       111570
   2   1    10.1489    8.70886     70   0.15020   6921        53958
   3   7    17.7158    5.00245     44   0.16410   4373        42788

# Peak Data List
      peak   2Theta      d        I/I1   FWHM     Intensity  Integrated Int
      no.    (deg)      (A)              (deg)    (Counts)   (Counts)
       1    10.1489    8.70886     70   0.15020   6921        53958
       2    11.4270    7.73749     21   0.16850   2117        21906
       3    12.6476    6.99337    100   0.18730   9851       111570
       4    13.7082    6.45459      9   0.16130    852         8293
       5    15.1829    5.83081     42   0.16350   4136        40584
       6    15.9876    5.53910     12   0.16090   1180        11586
       7    17.7158    5.00245     44   0.16410   4373        42788
       8    18.3101    4.84141      9   0.19790    840         9921
       9    18.9400    4.68179      6   0.15560    601         5178
      10    19.1798    4.62379      3   0.14000    316         2491
      11    19.8148    4.47702      6   0.18000    557         6653
      12    20.2911    4.37299     38   0.19830   3768        39060
      13    20.5800    4.31225      5   0.18480    503         6737
      14    22.8247    3.89299     24   0.18590   2400        23830
      15    23.0200    3.86040      6   0.10540    579         5118
      16    23.3592    3.80510      3   0.16600    327         5622
      17    25.0600    3.55058      4   0.21040    441         6697
      18    25.3304    3.51328     13   0.22610   1327        14866
      19    25.9078    3.43628     12   0.15280   1145         9798
      20    27.5816    3.23143      8   0.14830    753         6594
      21    27.9667    3.18780     12   0.18280   1209        13503
      22    29.1454    3.06151      4   0.31780    360         6058
      23    29.4600    3.02952      3   0.16100    338         3409
      24    29.8400    2.99180     10   0.20560    958         9232
      25    30.0200    2.97427      9   0.17440    922         7791
      26    30.6040    2.91883     30   0.16920   2995        29822
      27    30.8600    2.89520      4   0.00000    399            0
      28    31.0200    2.88063      4   0.17540    418         5775
      29    32.4519    2.75672      7   0.17090    643         8771
      30    33.1691    2.69874      6   0.18230    594         8671
      31    34.1815    2.62108      3   0.15390    338         3384
      32    34.6449    2.58708      7   0.17270    734         8910
      33    35.1891    2.54831      8   0.14740    748         6789
      34    35.8171    2.50505      5   0.23510    531         8230
      35    37.1760    2.41655      5   0.20700    458         5751
      36    37.7400    2.38172      5   0.16160    488         8508
      37    37.9600    2.36842      6   0.00000    574            0
      38    38.4244    2.34086      8   0.24580    777        14824
      39    38.7284    2.32318      6   0.19870    603         7277
      40    39.9115    2.25700     11   0.17130   1074        11204
      41    40.7030    2.21492      4   0.15250    378         3650
      42    41.1600    2.19137      7   0.23360    735         8267
      43    41.3400    2.18225     11   0.15600   1087         8369
      44    41.7554    2.16149      4   0.19740    403         4286
      45    42.1571    2.14182      5   0.20490    454         5313
      46    43.7974    2.06533      7   0.16970    665         7646
      47    44.7245    2.02465      3   0.17050    324         3776
      48    45.0174    2.01215      3   0.16850    327         3090
      49    45.2937    2.00052     10   0.14630   1016         8143
      50    46.5151    1.95079      5   0.18550    482         5977
      51    46.8795    1.93648     12   0.15750   1203         9934
      52    47.9456    1.89588      4   0.16870    416         5120
      53    49.1957    1.85059      4   0.21780    443         6281
```

peak no.	2Theta (deg)	d (A)	I/I1	FWHM (deg)	Intensity (Counts)	Integrated Int (Counts)
54	50.9007	1.79253	7	0.17450	664	9733
55	51.8378	1.76230	9	0.15380	850	9136
56	58.9189	1.56626	3	0.16430	321	3776
57	59.8075	1.54510	3	0.15350	324	3474
58	65.1364	1.43098	4	0.18680	381	4762

Figure B.1: Information for XRD analysis (I)

```
          ***  Basic Data Process  ***


# Data Infomation
        Group            : Standard
        Data             : TBY Set_3
        Sample Nmae      : Set_3
        Comment          :
        Date & Time      : 08-27-18 11:33:01


# Measurement Condition
    X-ray tube
        target           : Cu
        voltage          : 40.0 (kV)
        current          : 30.0 (mA)
    Slits
        Auto Slit        : not Used
        divergence slit  :   1.00000 (deg)
        scatter slit     :   1.00000 (deg)
        receiving slit   :   0.30000 (mm)
    Scanning
        drive axis       : Theta-2Theta
        scan range       :   10.0000 - 80.0000 (deg)
        scan mode        : Continuous Scan
        scan speed       :   2.0000 (deg/min)
        sampling pitch   :   0.0200 (deg)
        preset time      :   0.60 (sec)


# Data Process Condition
    Smoothing            [ AUTO ]
        smoothing points : 11
    B.G.Subtruction      [ AUTO ]
        sampling points  : 11
        repeat times     : 30
    Kal-a2 Separate      [ MANUAL ]
        Kal a2 ratio     : 50 (%)
    Peak Search          [ AUTO ]
        differential points : 11
        FWHM threhold    : 0.050 (deg)
        intensity threhold : 30 (par mil)
        FWHM ratio  (n-1)/n : 2
    System error Correction   [ NO ]
    Precise peak Correction   [ NO ]
```
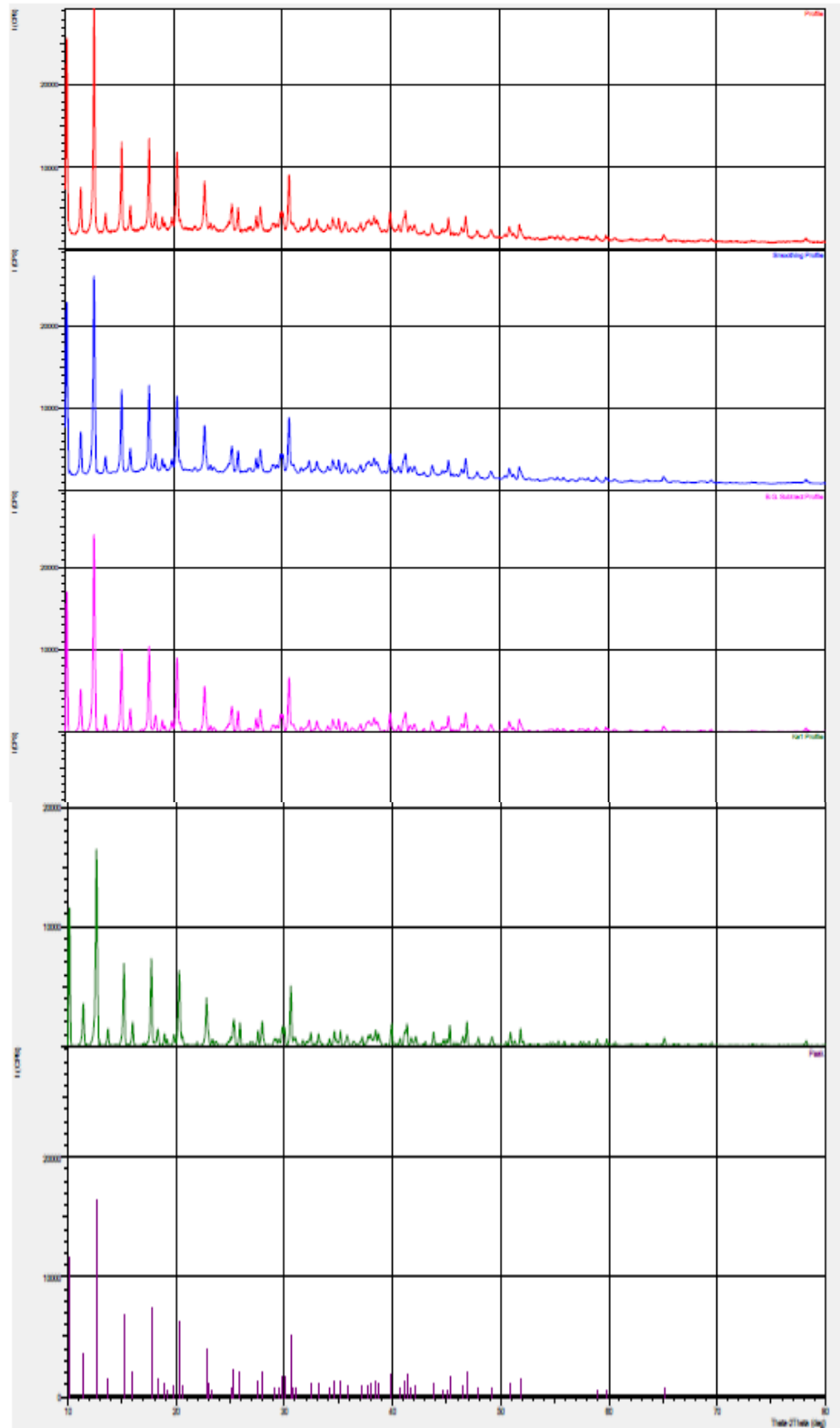
Figure B.2: Information for XRD analysis (II).

Figure B.3: Information for XRD analysis (III).

Match! Phase Analysis Report

Sample: Set_3 ()

Sample Data

File name	TBY_Set_3.ORG
File path	C:/xddat/Standard/TBY_Set_3
Data collected	Aug 27, 2018 12:09:56
Data range	9.910° - 79.910°
Number of points	3501
Step size	0.020
Rietveld refinement converged	No
Alpha2 subtracted	No
Background subtr.	No
Data smoothed	No
2theta correction	-0.09°
Radiation	X-rays
Wavelength	1.540600 Å

Candidates

Name	Formula	Entry No.	FoM
Silver	Ag	01-077-6577	0.7091

Search-Match

Settings

Reference database used	PDF-2 Release 2016 RDB
Automatic zeropoint adaptation	Yes
Minimum figure-of-merit (FoM)	0.60
2theta window for peak corr.	0.30 deg.
Minimum rel. int. for peak corr.	1
Parameter/influence 2theta	0.50
Parameter/influence intensities	0.50
Parameter multiple/single phase(s)	0.50

Selection Criteria

Elements:

Elements that must be present:	Ag
Elements that must NOT be present:	All elements not mentioned above

Peak List

No.	2theta [°]	d [A]	I/I0	FWHM
1	10.07	8.7781	676.53	0.1200
2	11.35	7.7889	180.46	0.1600
3	12.57	7.0342	1000.00	0.1600
4	13.64	6.4883	80.29	0.1600
5	15.11	5.8590	376.46	0.1600
6	15.91	5.5646	106.34	0.1200
7	17.64	5.0226	383.19	0.1600
8	18.24	4.8603	68.00	0.1600
9	18.87	4.6992	46.01	0.1600
10	19.74	4.4934	44.22	0.1200
11	20.22	4.3889	335.55	0.2000
12	20.51	4.3272	40.28	0.1600
13	22.75	3.9058	204.96	0.2000
14	24.78	3.5894	19.95	0.2000
15	24.98	3.5618	36.69	0.2000
16	25.27	3.5210	116.15	0.2400
17	25.84	3.4453	92.46	0.1600
18	27.51	3.2395	56.16	0.1600
19	27.90	3.1957	95.91	0.2000
20	29.01	3.0755	24.66	0.2000
21	29.42	3.0335	22.70	0.1600
22	29.76	2.9997	74.10	0.2400
23	29.95	2.9813	74.14	0.1600
24	30.54	2.9251	241.36	0.2000
25	30.93	2.8887	28.86	0.2000
26	32.39	2.7618	47.37	0.1200
27	33.10	2.7040	43.78	0.2000
28	34.11	2.6262	20.78	0.1600
29	34.57	2.5923	49.23	0.1600

30	35.12	2.5533	45.63	0.1200
31	35.74	2.5104	30.73	0.1600
32	37.13	2.4194	24.65	0.1600
33	37.89	2.3726	39.57	0.4000
34	38.37	2.3438	54.96	0.2000
35	38.66	2.3272	39.01	0.2800
36	39.85	2.2606	73.51	0.1600
37	41.05	2.1970	48.30	0.3200
38	41.26	2.1865	83.00	0.2400
39	41.69	2.1649	24.25	0.1200
40	42.09	2.1449	30.57	0.2000
41	43.73	2.0685	44.72	0.1600
42	44.65	2.0277	20.83	0.1200
43	44.95	2.0150	20.42	0.2800
44	45.22	2.0037	67.79	0.1600
45	46.45	1.9536	35.08	0.1600
46	46.80	1.9394	85.35	0.1600
47	47.87	1.8988	27.90	0.2400
48	49.14	1.8525	32.72	0.2800
49	50.82	1.7950	45.22	0.2400
50	51.20	1.7827	17.84	0.1600
51	51.76	1.7649	53.09	0.2000
52	65.02	1.4333	22.21	0.1600
53	78.17	1.2217	17.80	0.2000

Rietveld Refinement using FullProf

Calculation was not run or did not converge.

Crystallite Size Estimation using Scherrer Formula

Calculation was not run.

Integrated Profile Areas

Based on calculated profile

Profile area	Counts	Amount
Overall diffraction profile	4711440	100.00%
Background radiation	3670803	77.91%
Diffraction peaks	1040637	22.09%
Peak area belonging to selected phases	0	0.00%
Unidentified peak area	995268	21.12%

Peak Residuals

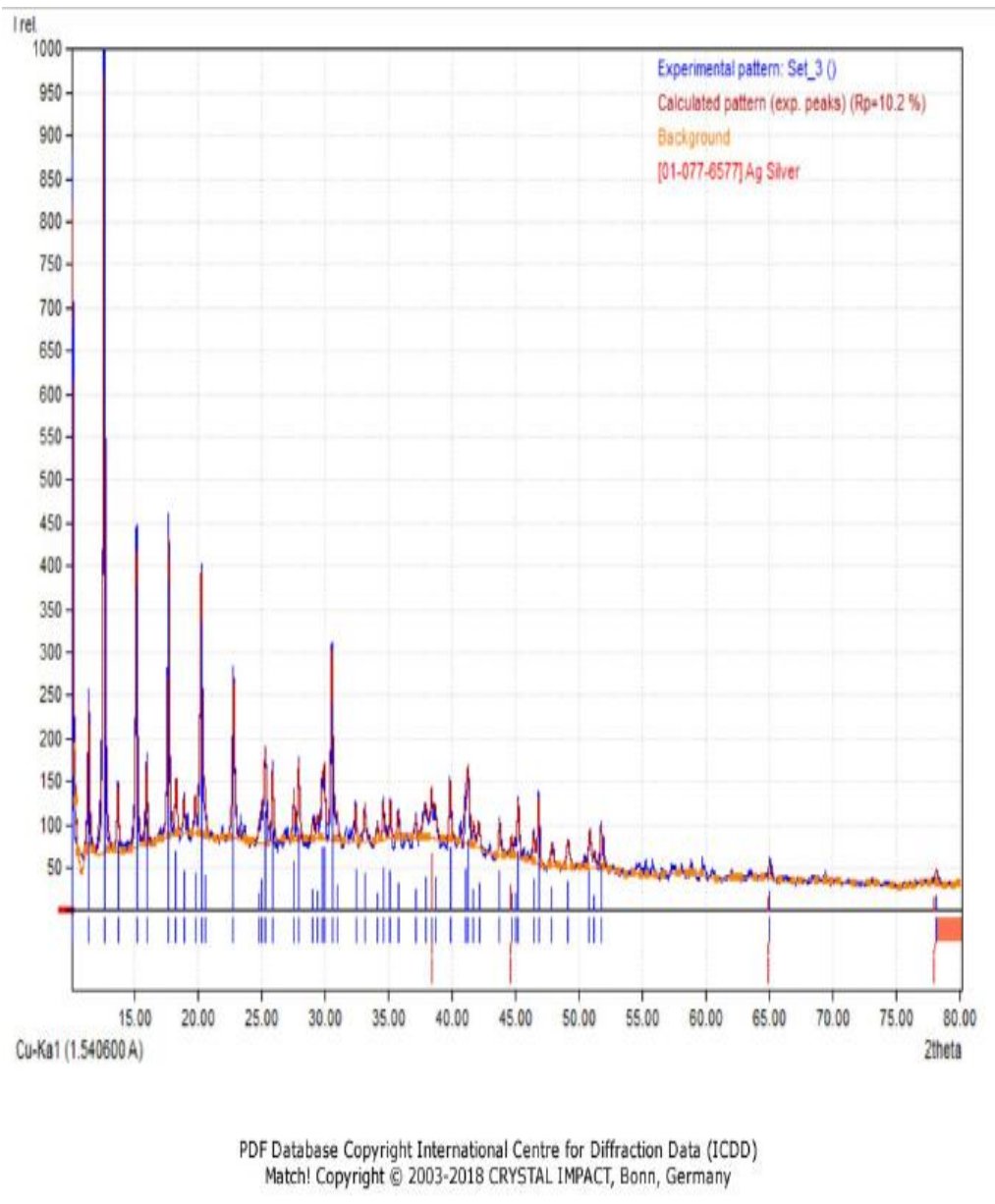| Peak data	Counts	Amount
Overall peak intensity	19891	100.00%
Peak intensity belonging to selected phases	15738	79.12%
Unidentified peak intensity	4152	20.88%

Diffraction Pattern Graphics

Figure C: Phase analysis report for XRD analysis.

Appendix D

Average size of synthesized AgNPs,

Calculation for β

$$\beta = \frac{\text{FWHM in } 2\theta \times \pi}{180\,°}$$

$$= \frac{0.2000 \times \pi}{180\,°}$$

$$= 3.491 \times 10^{-3}$$

Calculation for crystalline size by Debye–Scherrer equation

$$D = \frac{k\lambda}{\beta \cos\theta}$$

$$= \frac{(0.9) \times (1.5406 \times 10^{-10}\text{ m})}{(3.491 \times 10^{-3}) \cos 38.37}$$

$$= 5.066 \times 10^{-8}\text{ m} \times 10^{9}$$

$$= 50.66\text{ nm}$$

Where

D=Crystalline diameter

k= Scherrer's constant (value always is 0.9)

λ= Wavelength of X-ray source, Cu K_α radiation (1.5406 Å)

β= Width of diffraction broadening at full-width half maximum (in radian 2θ)

θ = Bragg's diffraction angle

Appendix E

Mass of centrifuge tube = 48.8576 g

Mass of centrifuge tube + AgNPs = 48.8646 g

Mass of AgNPs = 0.0070 g

The chemical equation of reduction of silver nitrate by sodium borohydride:

$$AgNO_3 + NaBH_4 \longrightarrow Ag + \frac{1}{2} H_2 + \frac{1}{2} B_2H_6 + NaNO_3$$

Due to excess amount of reducing agent was added, the silver nitrate was limiting agent in this case. From the chemical equation, it can be observed that one mole of silver nitrate will produce one mole of silver particles.

Theoretical value:

$$mole = \frac{mass}{molar\ mass} = Molarity\ x\ liters$$

Mole of silver nitrate used $= \frac{0.02\ M\ x\ 9\ mL}{1000} = 1.8\ x\ 10^{-4}$ mol

Molar mass of silver = 107.87 g/mol

$$mole = \frac{mass, g}{molar\ mass,\ g/mol}$$

Mass = molar mass (g/mol) x mole (mol)

$\quad$ = 107.87 g/mol x 1.8 x 10^{-4} mol

$\quad$ = 0.0194 g

$$percentage\ yield = \frac{actual\ mass, g}{theoretical\ mass, g}\ x\ 100\%$$

$$= \frac{0.0070\ g}{0.0194\ g}\ x\ 100\% = 36.05\%$$

The concentration of the AgNPs that were coated on the surface of solar cell,

0.02 M x 0.3605 = 7.21 x 10^3 M

Appendix F

$$Improvement\ percentage = \frac{Increment\ in\ power\ output}{Power\ output\ of\ bare\ solar\ cell}\ x\ 100\%$$

For S = 0.5, C.A. 5%,

$$Improvement\ percentage = \frac{0.248-0.125}{0.125}\ x\ 100\% = 98.40\ \%$$

For S = 1.0, C.A. 5%,

$$Improvement\ percentage = \frac{0.246-0.125}{0.125}\ x\ 100\% = 96.80\ \%$$

For S = 2.0, C.A. 5%,

$$Improvement\ percentage = \frac{0.259-0.125}{0.125}\ x\ 100\% = 107.2\ \%$$

For S = 3.0, C.A. 5%,

$$Improvement\ percentage = \frac{0.255-0.125}{0.125}\ x\ 100\% = 104.0\ \%$$

For C.A. 1%, S = 3.0,

$$Improvement\ percentage = \frac{0.217-0.125}{0.125}\ x\ 100\% = 73.60\ \%$$

For C.A. 3%, S= 3.0,

$$Improvement\ percentage = \frac{0.224-0.125}{0.125}\ x\ 100\% = 79.20\ \%$$

For C.A. 5%, S = 3.0,

$$Improvement\ percentage = \frac{0.255 - 0.125}{0.125} \times 100\% = 104.0\ \%$$

For C.A. 7%, S = 3.0,

$$Improvement\ percentage = \frac{0.261 - 0.125}{0.125} \times 100\% = 108.8\ \%$$

For C.A. 9%, S = 3.0,

$$Improvement\ percentage = \frac{0.251 - 0.125}{0.125} \times 100\% = 100.8\ \%$$

For C.A 11%, S = 3.0,

$$Improvement\ percentage = \frac{0.227 - 0.125}{0.125} \times 100\% = 81.60\ \%$$

For C.A. 13%, S = 3.0,

$$Improvement\ percentage = \frac{0.226 - 0.125}{0.125} \times 100\% = 80.80\ \%$$

For C.A. 15%, S = 3.0,

$$Improvement\ percentage = \frac{0.226 - 0.125}{0.125} \times 100\% = 80.80\ \%$$